TITLE:

Dynamic neuro-immune regulation of psychiatric risk loci in human neurons

AUTHORS:

Kayla G. Retallick-Townsley[1-2,4], Seoyeon Lee*[5,6], Sarah E. Williams*[4], Sam Cartwright**[1,4], Sophie Cohen**[1,4], Annabel Sen**[5,6], Meng Jia[5,6], Hannah Young[1,3], Lee Dobbyn[1-3], Michael Deans[5,6], Meilin Fernandez-Garcia[5,6], Laura M. Huckins[5#], Kristen J. Brennand[1,4,5,6#]

AFFILIATIONS

[1]Department of Genetics and Genomics, Icahn School of Medicine at Mount Sinai, New York, NY, USA.

[2]Icahn Institute of Genomics and Multiscale Biology, Icahn School of Medicine at Mount Sinai, New York, NY, USA.

[3]Pamela Sklar Division of Psychiatric Genomics, Icahn School of Medicine at Mount Sinai, New York, NY, USA.

[4] Nash Family Department of Neuroscience, Friedman Brain Institute, Icahn School of Medicine at Mount Sinai, New York, NY 10029

[5] Department of Psychiatry, Division of Molecular Psychiatry, Yale University School of Medicine, New Haven, CT 06511

[6] Department of Genetics, Wu Tsai Institute, Yale University School of Medicine, New Haven, CT 06511

*Contributed equally

#Co-corresponence: kristen.brennand@yale.edu and laura.huckins@yale.edu

ABSTRACT

The prenatal environment influences neurodevelopment and subsequent clinical trajectories for psychiatric outcomes in childhood and adolescence. Yet it remains unclear if the impact of maternal and fetal immune activation varies with distinct polygenic risk profiles. Therefore, here we catalogue genotype and environment (GxE) interactions, contrasting allele-specific regulatory activity between inflammatory contexts. We report a cue-specific neuronal massively parallel reporter assay (MPRA) of 220 loci from genome-wide association study (GWAS) linked to ten brain traits/disorders, empirically dissecting the impact of interleukin-6 (IL-6) and interferon-alpha (IFNα) on transcriptional activity. Of 1,469 active candidate regulatory risk elements (MPRA-active CRSs) across three conditions, we identify 316 with dynamic variant-specific effects (MPRA-QTLs) in human induced pluripotent stem cell (hiPSC)-derived glutamatergic neurons. Broadly, across hundreds of variants, neuronal immune-mediated regulatory activity is driven by differences in transcription factor binding and chromatin accessibility, the gene targets of which show pleiotropic enrichments for brain, metabolic, and immune disorders. Dynamic genetic regulation mediates immune effects, informing our understanding of mechanisms governing pleiotropy and variable penetrance. Understanding neurodevelopmental GxE interactions will inform mental health trajectories and resolve mechanisms mediating prenatal risk.

KEYWORDS

massively parallel reporter assay, human induced pluripotent stem cells, dynamic expression quantitative trait loci, psychiatric genetics, inflammation, immune signaling, fetal brain development

GLOSSARY OF TERMS:

CRE: The set of high-confidence candidate regulatory elements (e.g., promoters and enhancers) identified by ENCODE[1,2] and PsychENCODE BrainScope[3] resources.

MPRA sequences: All putative candidate regulatory sequences (CRS) from brain disease/trait GWAS prioritized for inclusion in the MPRA.

MPRA-active CRSs: The subset of candidate regulatory sequences (CRS) with significant transcriptional activity resolved by MPRA; MPRA-validated regulatory sequences.

MPRA-QTLs: The subset of MPRA-active CRS whereby single-nucleotide changes significantly altered transcriptional activity; MPRA-validated expression quantitative trait loci.

MPRA Dynamic-QTLs: The subset of MPRA-QTL single-nucleotide changes that significantly alter transcriptional activity in a differential or dynamic manner between contexts; MPRA-validated dynamic expression quantitative trait loci.

Introduction

Genome-wide association studies (GWAS) have linked hundreds of significant loci with risk for psychiatric traits[4-9] and neurodegenerative disease[10,11], the overwhelming majority of which are non-coding variants, common in the population-at-large, and thought to regulate the expression of one or more target genes[12]. Yet, pinpointing specific causal variants is complex, with true signal obscured by linkage disequilibrium patterns, and polygenic risk scores still incapable of reliably predicting individual outcomes[13]. Interactions between risk variants with each other[14,15] and the environment[16] may underlie the variable penetrance and expressivity of genetic risk for complex brain disorders.

Prenatal neurodevelopment represents a key window during which environmental exposures interact with genetic risk[17]. Maternal immunometabolic stressors (e.g., infection[18], trauma[19], immune dysfunction[20], obesity[21] and diabetes[22]) are associated with subsequent neuropsychiatric disorder risk in childhood and adolescence. High levels of maternal cytokines (e.g., interleukin-6 (IL-6)[23,24]) cause immune dysregulation in rodent offspring[24-26], concomitant with changes in neurodevelopment, gene expression, circuit function, and behavior[27-30]. IL-6 likewise impacts gene expression, neurogenesis, and neuronal activity in cultured human neural cells[31-33]. Likewise, fetal cytokines (e.g., type 1 interferons, including IFNα) mediate placental response to infectious agents but can cause a range of neurological and neurodevelopmental defects in human[34]; genetic interferonopathies present with similar abnormalities in brain development[35]. Yet, what remains unclear is the extent to which cytokine effects vary between individuals with distinct polygenic risk profiles.

Traditional genomic studies assume genetic risk to be static, and so map risk variants without consideration of how regulation of gene expression can change, but examples of cell-type-[36-38], sex-[39-41], and developmental stage-[42-45] specific, stress-[46,47], inflammation-[48,49], body mass index-[50], and drug-[51-53] dependent genetic regulation of gene expression abound. We hypothesize that the regulatory activity of non-coding risk variants in human neurons is influenced by inflammatory cues, and that resulting context-specific effects may alter susceptibility for complex brain disorders and diverse neurotypes. Which genetic variants show dynamic immune-responsive regulatory activity in neurons is unknown.

By coupling massively parallel reporter assays (MPRAs)[54,55] with human induced pluripotent stem cell (hiPSC) models[56-58], transcriptional activity can be empirically evaluated at scale in live human neurons. Here, we test the hypothesis that prenatal immune signaling (specifically IL-6 and IFNα) interact with non-coding regulatory elements by characterizing the dynamic transcriptional activity of 3,448 candidate regulatory sequences (CRSs) prioritized from 220 GWAS loci linked to ten brain traits/disorders. Altogether, we modelled dynamic immune contributions to neurodevelopment that precede symptom onset and disorder etiology by decades.

Results

Dynamic neuronal changes in response to immune signaling

Given that hiPSC-derived *NGN2*-induced glutamatergic neurons (iGLUTs)[59,60] most resemble their fetal counterparts[61], the influence of inflammatory cues during neurodevelopment was assessed using iGLUTs from two control donors that were acutely (24- and 48-hours) treated with IL-6 (60ng/mL), IFNα (IFNα-2b, 500 IU/mL), or vehicle (0.1% FBS in ultrapure H_2O) before harvesting at 24 days *in vitro* (DIV) (experimental schematic: **SI Fig. 1**). Treatment dose was informed by previous studies in human neural progenitor cells (NPCs) and neurons: IL-6[31,33], IFNα[62].

Receptors for all stressors (IL-6: *IL6R*, *IL6ST;* IFNα: *IFNAR1*, *IFNAR2*) were expressed in iGLUTs (**SI Fig. 2**). In classical IL-6 signaling, IL-6 binds to membrane-bound IL6R which then associates with glycoprotein 130 (GP130, encoded by *IL6ST*); comparatively, signaling via hyper-IL-6 delivers IL-6 covalently bound to soluble IL6R. Notably, no qualitative differences between classical and trans IL-6 signaling pathways have been reported[63]. Although others reported that, given low *IL6R* expression, hiPSC-derived NPCs do not respond to IL-6 and require hyper-IL-6 treatment[31,64], we find that iGLUTs increase *IL6R* expression with neuronal maturation (normalized *IL6R* expression was significantly higher in D24 iGLUTs compared to NPCs (Kruskal-Wallis, p=0.0056, pairwise Dunn's test p=0.0041) (**SI Fig. 2A**) and demonstrate robust neuronal transcriptomic, epigenomic, and cellular response to classical IL-6 signaling as follows.

In glia, different immune stressors induce distinct cellular states[65,66]; our findings indicate that this may likewise occurs in neurons (**SI Figs. 3-5**). There was limited overlap between either significant (BH-FDR-corrected p-value $p_{FDR}<0.05$) or nominally significant (unadjusted $p_{nom}<0.05$) differentially expressed genes (DEGs) by cue, with IL-6 treatment more moderately impacting the transcriptome (12 down-regulated and 1 up-regulated DEG, p_{FDR} <0.05: 1434 DEGs, $p_{nom}<0.05$) relative to IFNα treatment (39 down- and 97 up-regulated DEGs, p_{FDR} <0.05; 2000 DEGs, $p_{nom}<0.05$) (**SI Fig. 3A-B; SI Fig. 5A-B; SI Data 1.1-1.4**). Individual cytokine significant effects at 24 and 48 hours were highly correlated (IL-6: r=0.35, p=0.00; IFNα r=0.72, $p=5.7\times10^{-230}$) (**SI Fig. 3A-C**), albeit with differences in the magnitude of effect, consistent with a robust initial response followed by a subsequent attempt to return to homeostasis. Nominal IL-6 DEGs were enriched for processes largely related to cell adhesion, whereas IFNα response genes were enriched for antigen binding, protein ubiquitination, and as expected, interferon (-log(p)=9.02; z-score=2.287) and neuroinflammatory signaling (-log(p)=8.24) (**SI Fig. 3D-E; SI Fig. 5C; SI Data 1.7**).

Despite clear differences between IL-6 and IFNα response, DEGs ($p_{nom}<0.05$) shared enrichments for pathways related to stress and immune response (e.g. mTOR signaling [IL-6(-log(p)=3.7; IFNα (-log(p)=6.25] and EIF2 signaling [IL-6(-log(p)=10.2; IFNα (-log(p)=24.7)]) (**SI Fig. 5C**, **SI Data 1.7**) and well-recapitulated fetal mouse brain signatures associated with four models of prenatal immune activation (poly(I|C)[67] (**SI Fig. 5D)**. Likewise, neuronal immune DEGs had shared and unique enrichments for risk genes associated with brain and immune disorders (**SI Fig. 5E**). These similarities reflect a core set of convergent genes (258 down-regulated and 352 up-regulated) with perturbations in the same direction across all conditions (meta-analysis $p_{FDR}<=0.05$) (**SI Data 1.6**). Altogether, although neuronal immune responses were distinct between

exposures, convergent mechanisms and shared enrichments between IL-6 and IFNα response were also resolved.

Chromatin accessibility changes were greatest with IL-6 (675 differentially active regions (DARs); p_{FDR} <=0.05) and more modest with IFNα (12 DARs; p_{FDR} <=0.05) (**SI Fig. 6-8; SI Data 1.10-1.11**), unlike transcriptomic changes, which were greatest with IFNα. Despite this, for DEGs that overlapped with chromatin DARs, cue-responsive gene expression (average expression) and chromatin accessibility (ATAC peak score) were moderately correlated [IL-6 exposure: Pearson's Correlation Coefficient r=0.15, p=0.012; IFNα exposure: r=0.082, p=0.062)] (**SI Fig. 8A**). Comparative enrichment analysis revealed robust IL-6-specific enrichments for calcium-dependent signaling and O-linked glycosylation, whereas IFNα-specific enrichments for interferon signaling and synaptic transmission; both were enriched for actin/cadherin binding (**SI Fig. 8B-C**).

Phenotypically, neither stressor altered cell number or synaptic puncta density, but IL-6 increased the number of mature neurons (p_{bon}<0.01) and IFNα significantly increased neurite outgrowth (p_{bon}<0.001) in immature neurons (**SI Fig. 9**).

Altogether, multimodal evidence indicated that acute exposure to IL-6 and IFNα in mature iGLUTs resulted in distinct neuronal states.

Dynamic transcriptional regulation of allele-specific activity at GWAS loci in neurons

To test the extent that neuronal immune response altered genetic regulation of expression by disease-relevant loci, we designed a cross-disorder Lenti-MPRA[55] library integrating GWAS summary statistics from ten brain disorders, neurotypes, and traits (Alzheimer's disease (AD)[68], attention deficit hyper-activity disorder (ADHD)[69], anorexia nervosa (AN)[70], autism spectrum disorder (ASD)[71], bipolar disorder (BIP)[72], major depressive disorder (MDD)[73], obsessive compulsive disorder (OCD)[74], post-traumatic stress disorder (PTSD)[75], schizophrenia (SCZ)[4], and neuroticism (NEU-P)[76]) with post-mortem brain eQTLs[77] (coloc2[78] and PrediXcan[79]) (**SI Fig. 10; SI Data 2.1-2.7**). The number of single nucleotide polymorphisms (SNPs) selected per trait was dependent on the number of significant loci per GWAS (**SI Fig. 10C; SI Fig. 11A**). In addition to 100 scramble controls for use as a measure of basal activity of the minimal promoter, the following sets of benchmark variants were included: 310 empirical (positive: n=164 and negative: n=146) controls[80], and 88 GWAS controls (lack of colocalization or brain QTL regulation (pph3>0.9)). In total, we included 9,344 sequences (9,244 SNP-centered elements, 100 scrambles) representing 4,622 biallelic pairs (**SI Data 2.8-2.9**).

The library was transduced into mature iGLUTs (21 DIV), 24 hours later neurons were acutely exposed (48 hours) to IL-6 (60ng/mL), IFNα (500 IU/mL) or vehicle (0.1% FBS in ultrapure H_2O) before harvest at 24 DIV (two control donors, two biological replicates each, experimental schematic: **SI Fig. 1**). Given our previous analyses showing that stress (synthetic cortisol, 1000nM hCort) and trauma eQTLs were highly conserved (up to 50%) between hiPSC-neurons and post-mortem brain[46,47], we conducted a preliminary analysis in neurons treated with hCort; results are provided in supplementary information. Normalized log2(RNA/DNA) ratios quantified transcriptional activity. Following filtering, 2994, 2879, and 2898 CREs and 44-48 scramble sequences (2513 shared sequences, 44 shared scrambles, mean nbarcode/sequence =74) were resolved across baseline, IL-6, and IFNα respectively (**SI Fig. 11B-D; SI Data 2.10)**.

Within donor technical replicates were highly correlated based on DNA and RNA counts (Pearson's correlation coefficient r >= 0.99) and log2 (RNA/DNA) (r=0.63-0.89, mean r=0.79) (**Fig. 1A, SI Fig. 12, SI Data 2.10**). Mean transcriptional activity varied across immune cues and was lowest at baseline (MPRAnalyze[81]; Student's T-test: IL-6, $p=7.4x10^{-10}$; IFNα, p=0.0047) (**SI Fig. 13A**).

MPRA-active CRSs are defined as "MPRA-validated cis-regulatory sequences" and are measured as transcriptional activity exceeding the mean distribution of scramble controls in the same cellular context. 32-42% of MPRA sequences were transcriptionally active (baseline, 43%; IL-6, 42%; IFNα, 32%) (**Fig. 13B**). Activity of scramble and negative reference variants (empirical[80] or colocalization ph3>0.9) did not differ from each other (Student's t-test: p=0.71), but were significantly different from the positive reference variants[80] (Student's t-test; scramble-v-positive: p=0.016, negative-v-positive: p=0.0061) (**SI Fig. 13C**). MPRA activity had robust correlations by donor and replicate (**Fig. 14A**) and most overlapped with PsychENCODE single-cell excitatory CREs and with distal enhancer-like sequences as annotated by ENCODE CREs (**SI Fig. 14B-D**).

MPRA-QTLs are defined as "single-nucleotide (variant) changes that significantly altered transcriptional activity" and are measured as the difference between the activity of the reference allele and the alternative allele. Of the 711(IL-6), 707 (IFNα), and 753 (Base) biallelic MPRA sequences resolved (**SI Fig. 15A**), 5-11% (11.4% baseline, n=86; 5% IL-6, n=38; 5% IFNα, n=36) showed variant specific effects and were termed MPRA-QTLs (BH-FDR-corrected p-value $p_{FDR}<0.1$) **(Fig. 1Di; SI Fig.15B**). For subsequent analyses, a less strict moderate significance threshold (Storey's q-value q_{Storey} <=0.05) was applied, finding 23-35% of bi-allelic MPRA sequences to be MPRA-QTLs (35% baseline, n=261; 27% IL-6, n=189; 23% IFNα, n=158). Of note, in all cases, the proportion of positive benchmark variants (selected based on empirical differential variant activity[80]) that were MPRA-QTLs was significantly greater than the proportion of negative benchmark variants[80] (Student's T-test, p=0.017) (**Fig. 1B; SI Fig. 15C**). Moreover, the relative proportion of significant MPRA-QTLs for index SNPs was greater than for SNPs in high LD (>0.8) (**Fig. 1C; SI Fig. 15C; SI Data 2.11-2.14**). MPRA-QTLs resolved in iGLUTs were significantly correlated with those previously reported in human neural progenitor cells[57] (MPRA-QTL $p_{FDR}<0.1$ threshold at baseline: r=0.9, p=0.0055) (**SI Fig. 16; SI Data 2.15**) and across cues (q_{Storey} < 0.05: r=0.56-0.722-0.4, $p<2x10^{-7}$, $p_{FDR}<0.1$: r=0.85-0.96, $p<1x10^{-04}$) **(SI Fig. 17B).** Downstream analyses were performed on MPRA-QTLs with q_{Storey} <0.05.

MPRA dynamic-QTLs are defined as "single-nucleotide changes that significantly altered transcriptional activity in a differential manner between contexts", whereas **MPRA stable-QTLs** were consistent across cues. Most MPRA-QTLs were dynamic: 46% of MPRA-QTLs were termed "cue-specific" with significant activity in only one condition (baseline=109, IL-6=69, IFNα=49; $q_{Storey}<0.05$) (**Fig. 1Dii; SI Fig. 17A**), 9-12% were "immune-specific", having significant effects in the same direction in response to both IL-6 and IFNα, and 8-9% were "immune-responsive", having significant effects in at least two conditions, but with variable direction and magnitude of effect. Notably, only 14 dynamic-QTLs reversed the direction of baseline activity in immune cues (**Fig. 2A**). Reflecting our eQTL-based prioritization strategy (**SI Fig. 10A**), 47% of MPRA sequences overlapped with adult brain eQTLs (pFDR<=0.05). Of these, the majority of

MPRA-QTLs (q_{Storey}<=0.05) validated the direction of effect of brain eQTLs from fetal[82] (60-79%) and adult[77] (64-71%) cortex, particularly excitatory neurons[83] (50-61%) (**Fig. 2E-F; SI Fig. 17C-D**). Likewise, the effect sizes of concordant MPRA-QTLs were significantly correlated with eQTL betas, albeit greater for fetal cortex (0.72-0.77) and excitatory neurons (0.57-0.70), compared to the adult cortex (0.59-0.61) (**Fig. 2E-F; SI Data 2.16**). Overall, dynamic MPRA-QTLs were significantly correlated, even while demonstrating 46% cue-specificity, as variant-by-immune effects tended to vary in magnitude but not direction across inflammatory cues.

113 brain and trait GWAS loci were represented by 557 MPRA-QTLs successfully measured in each of baseline, IL-6, and IFNα conditions. Of these, 43 GWAS loci had variant-by-immune effects across all three states, whereas 26 GWAS loci were cue-specific; of these, 14 GWAS loci were unique to baseline, 5 to IL-6 exposure, and 8 to IFNα exposure **(Fig. 2B-C**). Whereas some top loci were stable across all conditions (e.g., rs61826812 on chromosome 1: baseline $p=6x10^{-4}$, IL-6 $p=4.3x10^{-5}$, IFNα $p=9.9x10^{-6}$, Wilcoxon Rank Sum Test ref-vs-alt allele), others were dynamically regulated by immune activation (e.g., rs73088112 on chromosome 3 active only with IL-6 (p=0.0011) and rs117843471 on chromosome 22 active only with IFNα ($p=7.1x10^{-6}$) (**Fig. 2D**). ~76% of loci contained at least one cue-specific MPRA-QTL. Overall, the top MPRA-QTL at a given GWAS loci frequently varied between immune contexts.

Variant-specific disruptions in transcription factor binding affinities are predicted to drive dynamic inflammatory-responsive regulation of psychiatric risk loci.

Many CRS regulate gene expression through the binding of sequence-specific transcription factors (TFs) to cognate motifs. TF binding is influenced by, amongst other factors, chromatin state of the genomic locus and affinities of the binding site[84]. Given that dynamic regulatory activity is driven by transcription factors (TFs)[38,46,47,85], we assessed cue-specific changes in chromatin accessibility and variant-specific changes in predicted TF binding affinities. First, we scanned MPRA-QTLs (q_{Storey} <=0.05) for allele-specific disruptions in predicted TF binding affinity (p_{FDR}<0.05) across 446 unique TFs expressed in mature iGLUTs (1573 motifs) (**Fig. 3**). Top positively correlated TF motifs varied across conditions and included expected TFs: IL-6 with interleukin-associated TFs (e.g., *CREB1* and *HSF1*); IFNα with interferon-binding receptors (e.g., *IRF1*) and STATs (e.g., *STAT3*); hCort with glucocorticoid receptors (e.g., *NR3C1*) (**SI Fig. 18A-B**). There was notable overlap between cue-specific TF motif enrichments, cue-responsive chromatin accessibility, and TF gene expression changes (**Fig. 3A; SI Fig. 18C**): for example, IL-6 (PAX7: r=0.85, p=0.001) and IFNα (STAT3: r=0.77, p=0.0099) (**Fig. 3B**). Across TFs, MPRA-QTL effects were significantly correlated with cue-responsive gene expression changes at 24-hours post cue exposure (**Fig. 3Ci**), a correlation that was strengthened after filtering for only those TFs with multi-omic support (e.g., IL-6: *SOX5, PBX1, TCF3,* and *CREB5*; IFNα: *IRF9, KLF4, ESRRA,* and *RUNX2*) (**Fig. 3Cii**). Comparative gene set enrichment analysis of the TFs implicated in regulating responses to IL-6 (n=50) and IFNα (n=39) (overlap=10 TFs) confirmed expected roles of interleukins, TGF-beta, and STAT signaling in immune response and also highlighted enrichments for neurodevelopment, cellular response to stress, transcriptional regulation, and chromatin organization (**Fig. 3D**). Overall, dynamic

regulation of GWAS risk loci in response to neuronal inflammation is driven both by variant-specific binding affinities and cue-specific changes in chromatin accessibility.

Immune-dynamic regulatory elements are enriched for psych-psych and psych-cardiometabolic pleiotropy.

Given the shared genetic risk factors between inflammatory diseases and neuropsychiatric traits, we posited that immune-specific genetically regulated transcription would have pleiotropic effects across multiple traits. Dynamic MPRA-QTLs in response to IL-6 and IFNα (-log10(q_{Storey})) were significantly positively associated with the total number of GWAS associations (**Fig. 4A**). In addition to being associated with multiple individual traits, many variants were significant in multi-trait or pleiotropic GWAS (e.g., IL-6 specific MPRA-QTLs were annotated for SCZ-metabolic pleiotropy and IFNα MPRA-QTLs were annotated for ADHD-SCZ pleiotropy) (**Fig. 4B; SI Fig. 19; SI Data 2.19**).

Target genes regulated by cue-specific MPRA-QTLs were predicted using an adapted activity-by-contact[86] model (STARE[87]) that incorporated enhancer activity (MPRA activity and donor- and cue-matched neuronal chromatin accessibility), contact (Hi-C contact frequency), and predicted TF binding affinities (**Fig. 4C)**. Enhancer-to-gene mapping generally replicated the original eGene predictions (MPRA-QTLs and coloc2: $p=2.12\times10^{-37}$; MPRA-QTLs and S-PrediXcan: $p=1.76\times10^{-48}$, hypergeometric test for enrichment), although the top ranked gene per variant often varied (when more than one was predicted) (**Fig. 4D**). The overall number of strong (top 5th percentile or ABC score=1) candidate genes were significantly correlated with multi-trait associations (**SI Fig. 19C**). MPRA-QTL gene targets were highly enriched for psychiatric disorder risk genes, including SCZ, BIP, and cross neuropsychiatric disorder pleiotropy (CxD) (MAGMA[88]), as well as common comorbid metabolic and immune syndromes (**Fig. 4E**). Notably, when specifically considering immune-dynamic MPRA-QTL gene targets (**SI Fig. 20; SI Data 2.20-2.21**), enrichments were stronger for ASD, neurological disorders, and non-brain disorders such as gastro-esophageal reflux disease and peptic ulcer disease **(Fig. 4E).**

Dynamic transcriptional regulation (MPRA-QTLs), chromatin accessibility (ATAC peaks), chromatin contact (Hi-C loops), and variant-specific predicted TF binding affinities combined to underlie the mechanisms of variant-by-immune activity amongst GWAS loci (**Fig. 5**). For example, *rs6940638* is a GWAS SNP as well as a stable MPRA-QTL (Wilcoxon Rank Sum Test; Base: p=0.041, IL-6=0.17, p=0.052) (**Fig. 5Ai**), with significantly reduced transcriptional activity when the alternative allele (G) is predicted to disrupt a SOX5 binding motif (**Fig. 5Aii**). Notably, whereas *rs6940638* is a brain eQTL mapped to *BTN2A/BTN3A3*[89], enhancer-to-gene mapping predicted stronger regulation 500KB upstream at *ABT1,* a deleterious gene associated with motor and neuromuscular disorders (MalaCards) and GWAS target gene associated with numerous psychiatric, metabolic, and inflammatory disorders (GWAS catalogue) (**Fig. 5B**). Across cues, 316 unique variants showed significant regulatory effects in at least one condition, with 112 being stable MPRA-QTLs mapped to 43 loci, and 204 being dynamic MPRA-QTLs mapping to 55 loci, with a mean of 3 stable MPRA-QTLs and 4 dynamic MPRA-QTLs per locus. The *FTCDNL1* locus falls under dynamic regulation by multiple MPRA-validated brain-eQTLs mapped to *FTCDNL1/TYW4*. One of which, rs769949, is a cue-specific MPRA-QTL (IL6: q_{Storey}=0.016) in an iGLUT-specific chromatin loop with predicted multi-gene regulation including *STAB2* (**Fig. 5C**).

Discussion

By testing the regulatory activity of 220 GWAS loci linked to brain diseases and traits across dynamic immune-regulated contexts in live human neurons, we modelled the impact of maternal immune activation during neurodevelopment, demonstrating gene x environment interactions of broad relevance to subsequent neuropsychiatric outcomes. Overall, we characterized effects at 112 GWAS loci, reporting 3448 CRSs in human neurons, including 2531 CRS shared across contexts. Our neuronal lenti-MPRA replicated MPRA-CRS reported in NPCs, validated brain eQTLs, and highlighted known risk-associated eGenes, and in doing so, expanded upon existing resources by incorporating dynamic regulatory activity. Of those GWAS loci empirically determined to show variant-specific effects (MPRA-QTLs), most revealed context-dependent effects (dynamic MPRA-QTLs). Strong correlations between variant-by-immune activity across cues indicated that dynamic effects tended to affect the magnitude but not the direction of the regulatory activity. Unexpectedly, immune MPRA-QTLs were more often annotated for multi-trait and pleiotropic GWAS, and their predicted gene targets likewise highlighted pleiotropic convergence across psychiatric disorders, extending to neurodegenerative disease, neurotypes, and cardiometabolic syndromes. These pleiotropic effects suggest that variant-by-immune activity may increase risk for disease by similar mechanisms across cytokines and tissues.

Fetal brain development is exquisitely sensitive to inflammatory insults throughout pregnancy[90], with both maternal[20] and fetal[90] immune dysfunction, as well as genetic defects resulting in type I IFN overproduction[91,92], linked to aberrant neurodevelopment and increased risk of psychiatric and neurological outcomes in offspring. We selected two cytokines, IL-6 and IFNα, based on evidence from animal models[23,24,93,94], cell culture[31-33,62], inflammatory biomarkers[95-97], brain imaging[98,99], and post-mortem brain analyses[29,100]. Altogether, for both cytokines, there is robust evidence that they act

directly on neurons; whereas maternal IL-6 accumulates in the placenta[101] and crosses the fetal blood brain barrier[102], IFNα is generated by most fetal cells in response to infection, including in the fetal brain[34]. Indeed, our *in vitro* neuronal gene expression and chromatin accessibility analyses well reproduced findings from *in vivo* maternal immune activation models.

Yet, even for a simple acute treatment paradigm, we observed time-dependent effects worth considering in subsequent studies of dynamic genetic regulation. First, *IL6R* and *IL6ST* expression rapidly increased within 24-hours of IL-6 treatment but declined nearly to baseline by 48-hours; likewise, *IFNAR1* and *IFNAR2* expression initially decreased following exposure to IFNα, with levels returned to baseline by 48-hours. These trends paralleled genome-wide effects; although gene expression signatures were strongly correlated across time points, there were fewer DEGs and clear decreases in the magnitude of effects over time, consistent with a rapid initial neuronal response to immune activation followed by a subsequent attempt to return to homeostasis (of note, mature iGLUTs were treated one time, without re-exposure). Transcription at 24-hours post-treatment correlated more strongly with MPRA effects measured at 48-hours. These dynamic patterns indicated that for genotype-by-environment studies, gene expression and chromatin accessibility changes should be monitored over time, allowing careful consideration of pseudotime effects in MPRA studies when dissecting mechanistic pathways impacted by context-dependent genetic regulation.

Patterns of gene expression also change over longer time periods across neurodevelopment[103,104] and aging[105], which may underly critical periods of heighted susceptibility to environmental stressors. Such changes presumably arise from differences in genetic regulation, reflecting shifting patterns of TF expression that mediate enhancer activity[106,107]. Age-specific eQTLs modify the functional impact of genetic risk throughout lifespan[40,108,109] and are particularly relevant given the variable age of onset of symptom presentation across psychiatric disorders. Design of our MPRA library prioritized eQTLs from the adult brain; although our MPRA was conducted in iGLUTs that more resemble fetal-like neurons, MPRA-QTLs showed significant concordance with both adult and fetal eQTLs. A variety of methods now exist to maintain[110,111] or accelerate[112-115] aging *in vitro*, which could be incorporated into future MPRAs, towards dissecting the dynamic functional impact of genetic risk across neurodevelopment, brain maturation, and aging to inform mapping of brain-related GWAS and facilitate precision medicine.

Notable technical limitations in MPRA design and methodology reduce the broad generalizability of our GxE analyses. First, reflecting the present state of GWAS, the variants tested were identified in exclusively European-ancestry data and excluded the MHC locus. Moreover, many recent publicly available GWAS remain underpowered, overall biasing the MPRA library towards specific disorders (e.g., eating disorders, PTSD and OCD had very few variants included). Second, technical limitations restricted CREs to short DNA fragments flanking prioritized variants, potentially omitting crucial portions of larger regulatory regions. Recent technological innovations in MPRA (e.g., tiling MPRA design[116]) should facilitate examination of more complex regulatory sequences moving forward. Third, although MPRA activity was highly correlated between donors at baseline (r=0.74, 0.67), inter-donor variability in cue-specific

transcriptional activity was less so, particularly for IFNα response (r=0.68, 0.44). We caution that donor genotype and polygenic context may influence functional genomics and warrants further exploration[117,118]. Fourth, as CREs were tested outside their endogenous context, results may not accurately inform regulatory activity of distal gene targets. Although new methods to integrate matched cue-specific epigenetic datasets refine predictions of gene targets of enhancer activity[86,119], further experimental validation through crisprQTL[120] or prime-editing[121] is warranted. Future studies of cue-specific GxE effects across additional variants, doses, longitudinal and recovery time-points, contexts, cell-types (particularly brain-specific immune cells), and ultimately within more physiologically relevant brain organoids via emerging single-cell MPRA methods[122], and across an expanded number of donors via village-in-a-dish approaches[123,124], will be crucial for further dissection of how immune activation during fetal development contributes to brain disorder risk.

The influence of pro-inflammatory environmental factors on brain-related regulatory elements may explain biological mechanisms through which immune signaling contributes to increased susceptibility for complex brain disorders. We identified hundreds of GWAS variants that confer greater susceptibility to complex brain disorders following developmental exposure to neuroinflammation and mapped context specific risk-associated genes, informing the influence of GxE interactions on prenatal risk across complex brain traits. Frequently, dynamic neuronal immune-response genetic regulation reflected the combinatorial effects of multiple functional variants within an individual GWAS loci, with distinct variants top ranked across neuroimmune states; in fact, loci with immune-specific genetically regulated transcription were enriched for pleiotropic effects across multiple traits. Likewise, downstream target genes of dynamic-MPRA-QTLs were uniquely enriched for complex brain disorders and common comorbid metabolic and immune syndromes. The clinical impact of resolving GxE interactions include preventative measures (including improved prenatal care, public policy to alleviate life stress, early life intervention for high-risk individuals) and care of current patients (for example, drug repurposing, patient stratification by immune status, personalized prescription). Overall, when attempting to understand the genetic mechanisms of variable penetrance and pleiotropy, with broad relevance across complex traits and disorders, it is critical to consider the impact of dynamic regulation of gene expression.

Methods

Lenti-MPRA library design across neuropsychiatric trait GWAS

A Lenti-MPRA[125] library was designed by statistical fine-mapping of ten GWAS: (Alzheimer's disease (AD)[68], attention deficit hyper-activity disorder (ADHD)[69], anorexia nervosa (AN)[70], autism spectrum disorder (ASD)[71], bipolar disorder (BIP)[72], major depressive disorder (MDD)[73], obsessive compulsive disorder (OCD)[74], post-traumatic stress disorder (PTSD)[75], schizophrenia (SCZ)[4], and neuroticism (NEU-P)[76]) using two complimentary methods incorporating dorsolateral prefrontal cortex (DLPFC)[77] expression quantitative trait loci (eQTLs): Bayesian co-localization (coloc2[78]) and transcriptomic imputation (S-PrediXcan[79]) (**SI Fig. 11A; SI Data 2.1-2.3**). For the

former, significant GWAS loci and Dorsolateral Pre-frontal Cortex (DLPFC)[77] eQTLs from the Common Mind Consortium (CMC) were tested for co-localization using a lenient significance threshold for GWAS loci ($p<1x10^{-6}$). The most probable causal eQTLs from moderately to highly colocalized loci (PPH4>=0.5) were selected, along with all SNPs in high LD (r^2 >= 0.9) (**SI Data 2.2-2.3**); controls for coloc2 prioritization were selected from significant BIP GWAS loci that (i) did not colocalize (PPH3 > 0.9) and (ii) were not significant CMC DLPFC eQTLs. For S-PrediXcan, all SNPs within the predictor models of Bonferroni-corrected significant ($p<4.64x10^{-6}$;(0.05/10786)) trait-associated S-PrediXcan genes (eGenes) and all SNPs in high LD (r^2 >= 0.8) with them were selected (**SI Data 2.4-2.5**).

Several strategies were applied to incorporate appropriate controls. First, scramble sequences (n=100) were added as negative controls. Only the scramble controls were used for normalization and as a measure of basal activity of the minimal promoter. For a point of comparison, two additional sets of benchmark variants were included. As empirical controls, 310 SCZ and AD GWAS SNPs producing the greatest (n=164) and least (n=146) transcriptional shifts in K562 chronic myelogenous leukemia lymphoblasts and SK-SY5Y human neuroblastoma cells[80] that overlapped with CMC DLPFC eQTLs were included to compare results of previously tested sequences. Third, to query the regulatory activity of significant GWAS loci lacking eQTL associations, we included 88 significant BIP GWAS SNPs that (i) did not colocalize (PPH4<0.1/PPH3>0.9) and (ii) were not significant CMC DLPFC eQTLs.

After accounting for SNPs identified through multiple strategies, and removal of SNPs with sequences containing restriction digest sites (AgeI/SfbI), we synthesized a library of 4,622 SNPs (9,244 variants), many of which overlapped with chromatin accessible peaks in the DLPFC and hiPSC-derived neurons, and 100 scramble controls. Oligonucleotides were synthesized by Agilent and cloned into the lenti-MPRA vector [55]. We performed a power analysis using designmpra[126] to determine size limitations of our MPRA; with 9244 SNPs, 50 barcodes per SNP, activity standard deviation of 1 (typical range = 0.3-2), and 4 replicates, the power of a t-test to detect differential variant shifts of 0.75 or greater (≥ 5 times as much mRNA per input DNA) at a Bonferroni corrected alpha=0.05 level is 100%.

Lenti-MPRA library preparation and viral titration: The MPRA library was generated according to published lenti-MPRA protocols with slight modifications[125]. Briefly, 200 base pair oligonucleotides flanking each prioritized SNP were synthesized by Agilent to create an MPRA library of 9,244 neuropsychiatric associated variants. The Agilent oligo pool was PCR amplified, and a minimal promoter and spacer sequence added downstream of the CRE. Amplified fragments were purified and amplified again for 15 cycles to add a random 15bp sequence to serve as a unique barcode. Barcoded fragments were inserted in the *Sbf*I/*Age*I site of the pLS-SceI vector (AddGene #13772) and then transformed into 10-beta competent cells (NEB, C3020) via electroporation. Bacterial colonies were grown overnight on Ampicillin-positive plates and midi-prepped for plasmid collection. The quality of the purified plasmid was evaluated by Sanger Sequencing of 16 colonies at random. CRE-barcode associations were identified by sequencing of the purified plasmid (MiSeq; paired-end; 15milion reads). 2nd-generation lentiviral packaging of the purified plasmid was performed by the viral core at Boston's

Children Hospital. To determine MOI and approximation of appropriate viral volume we infected day 14 iGLUTs (0, 1, 2, 4, 8, 10, 16, 32, 64 µL) with control lentivirus (pLS-SV40-mP-EGFP; AddGene #137724) and harvested for 48hrs later. Following DNA isolation, we performed qPCR to calculate the MOI based the relative ratios of genomic DNA to inserted viral DNA (after subtracting background noise caused by residual backbone DNA).

Cell-type deconvolution of postmortem DLPFC: We checked for the relative abundance of cell-type in the postmortem CMC DLPFC by performing cell-type deconvolution with the R package dtangle[127] and a single-cell expression reference panel from the cerebral cortex. In the CMC DLPFC, glutamatergic neurons make up the highest proportion of cells based on cell-type deconvolution.

NGN2-glutamatergic neuron induction from clonalized hiPSC lines for molecular experiments[59,60]: Clonal hiPSCs from two neurotypical donors of European ancestry with average schizophrenia PRS and no history of psychiatric diagnoses (#3182 (XX) and #2607 (XY)) were generated by lentiviral transduction with pLV-TetO-hNGN2-eGFP-Neo and lentiviral FUW-M2rtTA (Addgene #20342), followed by antibiotic selection and clonal expansion. Stably selected clones were validated to ensure robust cell survival, expression of fluorescent tags, and transgene expression. hiPSCs were maintained in StemFlex™ Medium (ThermoFisher #A3349401) and passaged with EDTA (Life Technologies #15575-020).

On day 1, medium was switched to non-viral induction medium (DMEM/F12 (Thermofisher, #10565018), 1% N-2 (Thermofisher, #17502048), 2% B-27-RA (Thermofisher, #12587010)) and doxycycline (dox) was added to each well at a final concentration of 1 µg/mL. At day 2, transduced hiPSCs were treated with 500 µg/mL G418 (Thermofisher, #10131035). At day 4, medium was replaced including 1 µg/mL dox and 4 µM cytosine arabinoside (Ara-C) to reduce the proliferation of non-neuronal cells. On day 5, young neurons were dissociated with Accutase Cell Detachment Solution (Innovative Cell Technologies, # AT-104), counted and seeded at a density of $1x10^6$ per well of a Matrigel-coated 12-well plate. Medium was switched to Brainphys neuron medium (Brainphys (STEMCELL, # 05790), 1% N-2, 2% B27-RA, 1 µg/mL Natural Mouse Laminin (Thermofisher, # 23017015), 10 ng/mL BDNF (R&D, #248), 10 ng/mL GDNF (R&D, #212), 500 µg/mL Dibutyryl cyclic-AMP (Sigma, #D0627), 200 nM L-ascorbic acid (Sigma, # A4403)). For seeding, 10 mM Thiazovivin (Millipore, #S1459), 500 µg/mL G418 and 4 µM Ara-C and 1 µg/mL dox were added. At day 6, medium was replaced with Brainphys neuron medium with 4 µM Ara-C and 1 µg/mL dox. Subsequently, 50% of the medium was replaced with fresh neuronal medium (lacking dox and Ara-C) once every other day until the neurons were harvested at D24.

Cue-Specific RNAseq **(SI Fig. 1, 2-5, 8; SI Data 1**): Briefly, mature iGLUTs (22 DIV), were acutely exposed (24 or 48 hours) to IL-6 (60ng/mL), IFNα (500 IU/mL), hCORT (48hr only; 1000nM), or vehicle (0.1% FBS in ultrapure H_2O for IL-6 and IFNα, 17.1 µM EtOH for hCORT) before harvest at 24 DIV (two control donors, three to four replicates per donor per cue/vehicle treatment; experimental schematic: **SI Fig. 1**).

Compound	**Solvent**	**Supplier**	**Product #**	**Conc.**

Human-recombinant IL-6	UltraPure H_2O	Sigma/Aldrich	GF338	60 ng/mL
Human-recombinant INFa2-b	UltraPure H_2O	Mount Sinai Pharmacy	NDC 0085-4350-01	500 IU/mL
Hydrocortisone	17.1 µM EtOH	Sigma/Aldrich	H0888	1000nM

RNA Sequencing libraries were prepared using the Kapa Total RNA library prep kit. Paired-end sequencing reads (100bp) were generated on a NovaSeq platform. Raw reads were aligned to hg38 using STAR aligner[128] (v2.5.2a) and gene-level expression were quantified by featureCounts[129] (v1.6.3) based on Ensemble GRCh38 annotation model. Genes with over 10 counts per million (CPM) in at least four samples were retained. Surrogate variable analysis (SVA) was performed to assess the correlation of known covariates and identify surrogate variables contributing to variance using the R packages sva[130] and variancePartition[131] (e.g. batch, treatment, donor, replicate, sex, and RIN). Following identification of SVs and covariates to correct for in the model, raw read counts were normalized with voom[102] and, due to the repeated measures study design, where individuals are represented by multiple independent technical replicates, differential expression analysis with repeated measures was performed by the *Dream* method from variancePartition[131]. Bayes shrinkage (limma::eBayes) estimated modified t- and p- values. Gene level significance values were adjusted for multiple testing using the Benjamini-Hochberg method to control the false discovery rate (FDR). Genes with FDR <□5% were considered significantly differentially expressed (limma::TopTable)[132] (**SI Data 1.1-1.5**). In these analyses, the t-test statistics from the differential expression contrast were used to rank genes in the GSEA using the R package ClusterProfiler[106] (**SI Data 1.7**). Gene-set enrichment analysis using WebGestalt[133] was performed between p_{nom}<0.05 DEGs and gene-sets curated from four rodent models of maternal immune activate: poly(I|C) exposure (conceptus, whole brain, amygdala, and frontal cortex)[27,67,134], IL-6 exposure (whole brain)[27], *H1N1* Flu virus infection (whole brain)[27], and chronic unpredictable maternal stress (whole brain)[135].

Meta-analysis of gene expression across cues. We performed a meta-analysis and Cochran's heterogeneity Q-test (METAL[136]) using the p-values and direction of effects (t-statistic), weighted according to sample size across all sets of perturbations (Target vs. Scramble DEGs). Genes were defined as convergent if they (1) had the same direction of effect across cue exposure (2) were Bonferroni significant in our meta-analysis (Bonferroni adjusted p-value; p_{Bon}<= 0.05), and (3) had a non-significant Cochran's Heterogeneity Test (**SI Data 1.6**).

Cue-Specific ATAC-Seq **(SI Fig. 1, 6-8; SI Data 1)***:* Briefly, mature iGLUTs (22 DIV), were acutely exposed (48 hours) to IL-6 (60ng/mL), IFNα (500 IU/mL), hCORT (1000nM), or vehicle (0.1% FBS in ultrapure H_2O for IL-6 and IFNα, 17.1 µM EtOH for hCORT) before harvest at 24 DIV (two control donors, two replicates per donor per cue/vehicle treatment; experimental schematic: **SI Fig. 1**). Mature neurons were washed with 500uL of PBS (-Ca/-Mg)-0.5mM EDTA per well of a 12-well plate. Then, 300uL dissociation solution (0.042 U/µL papain suspension (Worthington-Biochem LS003126) in HBSS (Thermofisher #14025076)-10mM HEPES (Thermofisher

#J61275AE)-0.5mM EDTA (Life Technologies #15575-020), pre-activated at 37C for 5 minutes) supplemented with 0.017U/µL DNase (Thermofisher #EN0521) and 1x Chroman I was added to each well before incubating the plate at 37C for 10 minutes, shaking at 125rpm. 600uL deactivating solution (DMEM-FBS-Chroman I) was then added to each well, and cells were dissociated into single cells by pipetting gently. For each condition, cells from 4 wells of a 12-well-plate were combined into a single 15mL conical tube for higher yield. After spinning at 600g for 5 minutes at room temperature, cells were resuspended in 310uL of DMEM (Thermofisher #10566-016)-10% FBS. Then, the cell suspension was filtered through a 37um reversible strainer and frozen in DMEM-10% FBS-10% DMSO.

ATAC sequencing library prep and sequencing were performed by the Yale Sequencing Core. The adaptor sequence for pair-end sequencing was removed using trim_galore[137] and sequencing quality measure by FastQC[138] and MultiQC[139]. Each experiment contained two technical replicates and two biological replicates (four samples total). All R1 and R2 fastqs passed basic QC with FastQC; total sequences per sample ranged from 47.2 million to 79.7 million after removal of mitochondrial reads (average 61M), with percent deduplicated ranging from 65%-80% (average 74.38%). Average GC content was normally distributed with a mean of 44% and average sequence length 85-119. Data was aligned with Bowtie2[140] against hg38 reference genome including rare SNVs. Mitochondrial reads were removed, sam files sorted and indexed, and converted to compressed BAM files with samtools[141]. Peak calling and reproducibility analysis were performed using MACS2 (2.1.0)[142] and IDR (version, soft-idr-threshold 0.05)[143] respectively, according to ENCODE ATAC-seq pipeline (v1 2019)[144] specifications. Fraction of reads in peaks (FRiP) scores were calculated for each sample from the alignment file (bam) and MACS2 narrowPeak files: FRiP scores ranged from 0.21-0.27 (**SI Data 1**), passing ENCODE ATACseq data standards (**SI Data 1.8**). All replicates passed the two ENCODE standards for IDR, with ratio of pooled pseudoreplicate results to true replicate results (Np/Nt) as well as self-replicate peaks (N1/N2) within a factor of two. Self-consistency ratio: max(N1,N2)/ min(N1,N2) = 1.56-2.86; and Rescue Ratio: max(Np,Nt)/ min(NP,Nt)=1.32-1.64 (**SI Data 1.8**). Consensus peak sets were defined as ATAC peaks present in at least 4 out of 6 pairwise true-replicate IDR comparisons for each condition (4 samples total), with at least 50% overlap (bedtools intersect -wa -u -f 0.50) resulting in a range of 19,373-27,930 peaks per condition. A single merged file was generated for each condition for visualization purposes by merging bam files with samtools, then intersecting that file with the list of consensus peaks via bedtools intersect. Bed files for each merged peak were opened with Integrative Genomics Viewer (IGV_2.16.0)[145] for figure generation. Separate narrowpeak files for each ATAC replicate were also intersected with the list of consensus peaks per condition to be used for differential accessibility analysis with DiffBind[146]. Counts for all replicates across conditions were normalized to full library size, donor was used as a blocking factor, treating within donor replicates as repeated measures, condition-vehicle comparisons were defined as individual contrasts, and differential sites for each contrast calculated using edgeR at a threshold of Benjamin-Hochberg method of multiple testing correction; $p_{FDR}<0.1$, or a nominal p-value <0.05 for subsequent analysis. Transcription factor binding site motif enrichment was performed using Homer (findMotifsGenome.pl -size given -mask) on differential accessible regions identified at both significance

thresholds[147]. Peak annotation was performed using ChIPseeker[148] (v 1.8.6) and gene set over representation analysis of genes mapped to open chromatin regions was performed with ClusterProfiler[149] using Gene Ontology, WikiPathway, KEGG, and REACTOME gene-sets.

Cue-specific MPRA (**SI Fig. 1, 10-20; SI Data 2)**: Briefly, the MPRA library was transduced into mature iGLUTs (21 DIV), 24 hours later neurons were acutely exposed (48 hours) to IL-6 (60ng/mL), IFNα (500 IU/mL) or vehicle (0.1% FBS in ultrapure H_2O) before harvest at 24 DIV (two control donors, two biological replicates each, experimental schematic: **SI Fig. 1**). Day 21 iGLUTs were spinfected (1krcf for 1 hr @37C, slow accel, slow deceleration) with lenti-MPRA library, (based on titrations of the control virus from the Gordon et al. 2020 lenti-MPRA Nature Protocol Supplement). 24 hours after spinfections, full media was replaced to remove un-integrated virus. At 48 hours post-infection, iGLUTs were treated with stress and inflammatory cues or basal media. The number of cells required pre-replicate was calculated according to the Gordon et al. 2020 protocol, with on average, 6 million hiPSCs seeded per replicate. 72hrs post-lentiviral-infection, and 48 hours post-exposure to stress or inflammatory compounds neuronal cells were washed three times and harvested using AllPrep DNA/RNA mini kit (Qiagen) and the libraries prepped as previously described. The libraries were sequenced as paired end reads on a NextSeq 2x50 on S2 flow cell (3.3-4.1 B reads/cell) by the New York Genome Center.

Lenti-MPRA CRS-barcode association from MiSeq. Sequencing of purified plasmid DNA was sequenced on an Illumina MiSeq v.2 (15 million paired-end reads_and generated fastq files with bcl2fastq (parameters: --minimum-trimmed-read-length 0 --mask-short-adapter-reads 0). Barcode-CRE association was performed as previously described using the association utility of MPRAflow v2.3.5[125] (run as: nextflow run association.nf –fastq-insert –fastq-bc –fastq-insertPE –mapq 1 –baseq 15).

Lenti-MPRA RNA/DNA counts. We demultiplexed the indexed DNA and RNA libraries and generated paired-end fastq files with bcl2fastq v2.20 and used the count utility of MPRAflow 2.3.5 both with and without the --mpranalyze flag included (run as: nextflow run count.nf -w –experiment-file –dir –outdir –labels –design –bc-length 14 –umi-length 16 --thresh 10) to compute the activity score for each element and produce count files formatted for analysis with MPRAnalyze[81]. The inserts were required to have at least 10 unique barcodes.

Lenti-MPRA comparison of regulatory activity across replicates, donors, and cue exposures. Across conditions 3,440-3747 of CREs were captured (minimum requirement of 10 barcodes each). Transcriptional activity, measured as the normalized log2 DNA and RNA counts per CRS, across conditions was strongly correlated between replicates (Pearson's Correlation Coefficient r=0.98-1.00; **SI Fig. 12**). However, normalized log2(RNA/DNA) ratios moderately correlated (mean r=0.45, max r=0.86), correlations in two sets of replicates were strongly affected by outlier sequences, largely effected by between-donor variability in sequences with low DNA counts and likely poor integration.

To improve the reproducibility of our results, we removed CRSs with (i) less than 10 barcodes and (ii) that did not replicate between technical replicates using outlier testing.

Many of the sequences that did not replicate had low DNA counts, likely indicating poor integration. Sequences that had low correlations between replicates were removed by calculating the difference in RNA/DNA ratio between replicates for each insert and identifying outliers in R using rstatix::identify_outliers with values above Q3 + 1.5x IQR or below Q1 - 1.5x IQR. Following filtering 2994-2879 sequences were retained, of which 2531 were MPRA-CRSs and 44 were scramble sequences. With the removal of CRSs whose effects were not reproducible, the correlations between log2 RNA/DNA ratio between technical replicates were highly correlated, (range 0.63 to 0.89) with an average correlation of 0.79, with only 1 comparison (donor 2607 following IFNα exposure below a correlation of 0.74; at 0.63) (**SI Fig. 12; SI Data 2.10**). Mean log2 normalized RNA/DNA ratios were moderately correlated between within batch donor replicates (r=0.46-0.75, mean=0.64). Full correlations between replicates are reported in. Across these sequences the number of barcodes per unique CRS were highly correlated between CRS shared across all conditions (r=0.997-0.999). There was no significant difference in mean number of barcodes (n~74) per insert or the proportion of CRS by prioritization method or disorder association across the conditions (**SI Fig. 13**).

Lenti-MPRA quantification. Mean transcriptional activity across replicates was calculated using MPRAnalyze. First, library size correction factors were estimated across replicates and donors using MPRAnalyze::estimateDepthFactors(obj, lib.factor=c("replicate","donor",) which.lib="both", depth.estimator="upper quantile"). Activity was quantified using MPRAnalyze::analyzeQuantification (obj = obj, dnaDesign = ~ donor + replicate, rnaDesign = ~ donor + replicate). Alpha values representing the transcriptional rate of each sequence were extracted from the fitted model MPRAnalyze::getAlpha. CRE were labeled active if their alpha value was above the median of the scramble controls sequences – which represent basal activity of the minimal promoter.

Lenti-MPRA variant-specific differential analysis. First, RNA/DNA counts were separated by reference and alternative alleles and merged. Library size correction factors were estimated across replicates and donors using MPRAnalyze::estimateDepthFactors(obj, lib.factor=c("replicate","donor") which.lib="both", depth.estimator="upper quantile"). Differential activity was calculated between alternate (alt) and reference (ref) alleles using the classic mode version of MPRAnalyze::analyzeComparative(mpraobject, dnaDesign = ~ replicate + donor + variant + barcode, rnaDesign= ~ variant, reducedDesign= ~ 1, mode="classic") and MPRAnalyze::testLrt(obj). Multiple testing correction was performed and sequences with an allelic-effect q_{Storey}<=0.05 were considered significant and designated as "MPRA-QTLs" (**SI Data 2.11-2.14**).

Lenti-MPRA cue-specific differential analysis. First, conditions were merged based on shared sequences and library size correction factors were estimated across replicates, donors, and conditions using MPRAnalyze::estimateDepthFactors(obj, lib.factor=c("replicate","donor","cue") which.lib="both", depth.estimator="upper quantile"). Differential activity analysis between IL-6, IFNα, hCORT exposure and baseline (media vehicle) was performed using MPRAnalyze::analyzeComparative(mpraobject, dnaDesign= ~ replicate + donor + cue, rnaDesign= ~cue, reducedDesign= ~ 1, correctControls=TRUE) and MPRAnalyze::testLrt(obj).

Analysis of allelic shifts in MPRA activity and comparison to eQTL datasets. We first assessed the absolute overlap of all MPRA sequences post filtering and bulk adult PFC[77], fetal brain[82], and the CMC adult DLPFC eQTLs. For overlapping MPRA-QTLs and eQTLs, we defined the percent concordant as the number of significant overlap SNPs with the same direction of effect in the MPRA-QTL and eQTL over the total number of overlapping SNPs. We calculated the Pearson's Correlation Coefficient (r) between MPRA-QTL logFC and eQTL betas from post-mortem single-cell[83] and bulk adult PFC[77], and fetal brain[82].

Overlap of MPRA-active sequences with cis CRE ENCODE annotations and brainSCOPE single cell atacCREs. We assessed overlap of active MPRA-CRSs with previously annotated cis-CREs across the human genome (hg38) from the Encode Registry[150,151] and with brainSCOPE[3] single-cell CREs defined based on chromatin accessibility peaks in brain cells from the adult PFC. Overlap was identified between ENCODE and brainSCOPE annotated bed files and the 200bp MPRA sequences using bedtools (bedtools intersect -wao).

Variant-specific predicted binding affinity scoring with atSNP and MotifBreakR. To identify TF that may influence GxE interaction related to stress, performed we motif affinity testing for SNPs with significant allelic shifts as measured by lenti-MPRA (MPRA-QTLs) using atSNP[152]. ENCODE derived TF motif binding PWM matrices were loaded and filtered for TF with expression in D24 iGLUTs, leaving 1573 motifs across 516 TFs. Genomic context (30bp half window size) of significant MPRA-QTLS (Storey's q-values q_{Storey} <=0.05) for each condition were pulled with atSNP::LoadSNPData. SNP allele affinity scores were calculated for each motif with atSNP::ComputeMotifScore and p-values computed using atSNP::ComputePValues. Rank p-values were used to assess the significance of the SNP effect on the affinity change. Bonferroni multiple testing correction was performed along with calculation of Storey's q-values and local FDR. Motif with significant SNP effects were tested for TF enrichments using hypergeometric tests with multiple testing correction across the total number of TFs tested. To identify TFs with binding patterns that predict variant-specific activity, SNP-motif pairs were filtered based on q_{Storey}<0.05. Pearson's Correlation Coefficients (r) were then calculated between MPRA-QTL activity (ref-vs-alt) and the logOdds that the reference allele enhanced affinity binding was assessed for each motif. To visualize allelic effects on predicted TF binding affinities for specific MPRA-QTLs, we used the motifbreakR package[153], filtered for strong allelic effects of TFs expressed in DIV24 iGLUTs.

Activity-by-Contact prediction of cue-specific regulatory element target genes. To predict target genes of condition-specific enhancer activity, we scored enhancer-gene interaction using STARE[87]. STARE combines an adapted Activity-By-Contact (ABC)[86] interaction modeling with predicted TF binding affinities in regions to summarize these affinities at the gene level. For each condition, we filtered significant MPRA-QTL (q_{Storey}<0.05) or nominally significant dynamic-MPRA-QTL (p_{nom}<0.05) for overlap with matched cue-specific chromatin accessibility peaks (p_{nom}<0.05) in iGLUTs. Enhancer "activity" for these variants was then calculated as the abs(logFC) compared to the alternative allele or baseline respectively, multiplied by the scaled peak AUC, thus incorporating crucial information about proximal cue-specific chromatin activity. Distal chromatin "contact" was measured from Hi-C data in iGLUTs[154], which include one

overlapping donor (2607). Genes were initially filtered by ABC score > 0.02 (default), but more stringent filtering was performed based on ABC score median thresholds prior to downstream enrichment analysis.

Over-representation analysis and biological theme comparison of correlated TFs and ABC genes. To identify pathway enrichments unique to cue-specific regulatory activity, we performed biological theme comparison using ClusterProfiler[149] and gene set enrichment for GWAS catalogue risk genes using the GENE2FUNC query tool of FUMA GWAS[155].

Enrichment analysis of convergence for risk loci using MAGMA. We tested ABC genes for enrichment with genetic risk of psychiatric, neurological, cardiometabolic, and immune disorders/traits [*Psychiatric*: attention-deficit/hyperactivity disorder (ADHD)[69], anorexia nervosa (AN[156], including binge-purge AN-BP and restrictive subtypes AN-R[157]), autism spectrum disorder (ASD)[6,158], alcohol dependence (AUD)[159], bipolar disorder (BIP, BIP-I, BIP-II)[72] cannabis use disorder (CUD)[160], major depressive disorder (MDD)[73], obsessive-compulsive disorder (OCD)[74], post-traumatic stress disorder (PTSD)[161], and schizophrenia (SCZ)[4], Cross Disorder (CxD)[162], Tourette's[163], and neurotic personality traits[76]; *neurologic*: Alzheimer disease (AD)[68], Parkinson disease (PD)[164], amyotrophic lateral sclerosis (ALS)[165], Multiple Sclerosis (MS)[166], Epilepsy (Epi)[167], migraine[168], chronic pain[169]; *Inflammatory-Gastrointestinal*: Diverticular Disease (DivD)[170], Gastro-oesophageal reflux disease (GORD)[170], Peptic Ulcer Disease (PUD)[170], Inflammatory Bowel Disease (IBD)[170], Irritable Bowel Syndrome (IBS)[170]; *Cardiometabolic*: Type-I Diabetes (T1D)[171], Type-2 Diabetes (T2D)[172], Metabolic Syndrome (MetS)[173], Atrial Fibrillation (Afib)[174], hypertension (HyperTen)[175]. *Anthropometric:* Body Mass Index (BMI)[176], left-handedness (left hand)[177] GWAS summary statistics] using multi-marker analysis of genomic annotation (MAGMA)[88]. SNPs were mapped to genes based on the corresponding build files for each GWAS summary dataset using the default method, snp-wise=mean (a test of the mean SNP association). A competitive gene set analysis was then used to test enrichment in genetic risk for a disorder across gene sets with an $p_{FDR}<0.05$.

iGLUT neuron induction from non-clonal hiPSC-derived NPCs for phenotypic assays[59,60]. hiPSCs-derived NPCs were dissociated with Accutase Cell Detachment Solution (Innovative Cell Technologies, #AT-104), counted and transduced with rtTA (Addgene 20342) and *NGN2* (Addgene 99378) lentiviruses in StemFlex media containing 10 mM Thiazovivin (Millipore, #S1459). They were subsequently seeded at $1x10^6$ cells/well in the prepared 6-well plate. On day 1, medium was switched to non-viral induction medium (DMEM/F12 (Thermofisher, #10565018), 1% N-2 (Thermofisher, #17502048), 2% B-27-RA (Thermofisher, #12587010)) and doxycycline (dox) was added to each well at a final concentration of 1 µg/mL. At day 2, transduced hiPSCs were treated with 500 µg/mL G418 (Thermofisher, #10131035). At day 4, medium was replaced including 1 µg/mL dox and 4 µM cytosine arabinoside (Ara-C) to reduce the proliferation of non-neuronal cells. On day 5, immature NPC-iGLUTs were dissociated with Accutase Cell Detachment Solution (Innovative Cell Technologies, #AT-104), counted and seeded at a density of $1x10^6$ per well of a Matrigel-coated 12-well plate. Medium was switched to Brainphys neuron medium (Brainphys (STEMCELL, # 05790), 1% N-2, 2% B27-RA, 1 µg/mL Natural Mouse Laminin (Thermofisher, # 23017015), 10

ng/mL BDNF (R&D, #248), 10 ng/mL GDNF (R&D, #212), 500 µg/mL Dibutyryl cyclic-AMP (Sigma, #D0627), 200 nM L-ascorbic acid (Sigma, # A4403)). For seeding, 10 mM Thiazovivin (Millipore, #S1459), 500 µg/mL G418 and 4 µM Ara-C and 1 µg/mL dox were added. At day 6, medium was replaced with Brainphys neuron medium with 4 µM Ara-C and 1 µg/mL dox. Subsequently, 50% of the medium was replaced with fresh neuronal medium (lacking dox and Ara-C) once every other day until the NPC-iGLUTs were harvested at d21.

Neurite analysis: Day 7 NPC-iGLUTs were seeded as $1.5x10^4$ cells/well in a 96-well plate coated with 4x Matrigel at day 3 followed by half medium changes until the neurons were fixed at day 7. At day 5, NPC-iGLUTs were treated for 48hrs with either hCort (1000nM), IL-6 (60 ng/mL), INFa-2b (500 IU/mL), or matched vehicles. Following cue exposure, NPC-iGLUTs were fixed using 4% formaldehyde/sucrose in PBS with Ca^{2+} and Mg^{2+} for 10 minutes at room temperature (RT). Fixed cultures were washed twice in PBS and permeabilized and blocked using 0.1% Triton/2% Normal Donkey Serum (NDS) in PBS for two hours. Cultures were then incubated with primary antibody solution (1:1000 MAP2 anti chicken (Abcam, ab5392) in PBS with 2% NDS) overnight at 4°C. Cultures were then washed 3x with PBS and incubated with secondary antibody solution (1:500 donkey anti chicken Alexa 647 (Life technologies, A10042) in PBS with 2% NDS) for 1 hour at RT. Cultures were washed a further 3x with PBS with the second wash containing 1 µg/ml DAPI. Fixed cultures were then imaged on a CellInsight CX7 HCS Platform with a 20x objective (0.4 NA) and neurite tracing analysis performed using the neurite tracing module in the Thermo Scientific HCS Studio 4.0 Cell Analysis Software. 12 wells were imaged per condition across two control donor hiPSCs, with 9 images acquired per well for neurite tracing analysis. A one-way ANOVA with a post hoc Bonferroni multiple comparisons test was performed on data for neurite length per neuron using Graphpad Prism.

Synapse analyses: Commercially available primary human astrocytes (pHAs, Sciencell, #1800; isolated from fetal female brain) were seeded on D3 NPC-iGLUTs at $1.7x10^4$ cells per well on a 4x Matrigel-coated 96□W plate in neuronal media supplemented with 2% fetal bovine serum (FBS). NPC-iGLUTs were seeded over the astrocyte monolayer as $1.5x10^5$ cells/well at day 5 post induction. Half changes of neuronal media were performed twice a week until fixation. At day 13, NPC-iGLUTs + astrocyte co-cultures were treated with 200 nM Ara-C to reduce the proliferation of non-neuronal cells in the culture. At day 18, Ara-C was completely withdrawn by full medium change followed by half medium changes until the neurons were fixed at day 21. At day 21, NPC-iGLUTs + astrocytes co-cultures were treated for 48hrs with hCort (1000nM), IL-6 (60 ng/mL), IFNα-2b (500 IU/mL), or matched vehicles. Following exposure, NPC-iGLUTs were fixed and immune-stained as described previously, with an additional antibody stain for Synapsin1 (primary antibody: 1:500 Synapsin1 anti mouse (Synaptic Systems, 106 011); secondary antibody: donkey anti mouse Alexa 568 (Life technologies A10037)). Stained cultures were imaged and analyzed as above using the synaptogenesis module in the Thermo Scientific HCS Studio 4.0 Cell Analysis Software to determine SYN1+ puncta number, area, and intensity per neurite length in each image. 20 wells were imaged per condition across two control donor hiPSCs, with 9 images acquired per well for synaptic puncta analysis. A one-way ANOVA with a post hoc Bonferroni multiple

comparisons test was performed on data for puncta number per neurite length using Graphpad Prism.

Antibody	Species	Supplier	Product #	Dilution
MAP2	Ck	Abcam	ab5392	1:500
SYNAPSIN1	Ms	Synaptic Systems	106 011	1:500
Alexa 568 anti-Mouse	Ms	Life technologies	A10037	1:500
Alexa 647 anti-Chicken	Ck	Life technologies	A10042	1:500

Multiple Electrode array (MEA): Commercially available primary human astrocytes (pHAs, Sciencell, #1800; isolated from fetal female brain) were seeded on D3 NPC-iGLUTs at $1.7x10^4$ cells per well on a 4x Matrigel-coated 48W MEA plate (catalog no. M768-tMEA-48W; Axion Biosystems) in neuronal media supplemented with 2% fetal bovine serum (FBS). At D5, iGLUTs were detached, spun down and seeded on the pHA cultures at $1.5x10^5$ cells per well. Half changes of neuronal media supplemented with 2% FBS were performed twice a week until day 42. At day 13, NPC-iGLUT + astrocyte co-cultures were treated with 200 nM Ara-C to reduce the proliferation of non-neuronal cells in the culture. At Day 18, Ara-C was completely withdrawn by full medium change. At day 26, NPC-iGLUTs + astrocytes co-cultures were treated for 48hrs with hCort (1000nM), IL-6 (60 ng/mL), IFNα-2b (500 IU/mL), or matched vehicles. Following exposure, electrical activity of iGLUTs was recorded at 37°C using the Axion Maestro MEA reader (Axion Biosystems). Recording was performed via AxiS 2.4. Batch mode/statistic compiler tool was run following the final recording. Quantitative analysis of the recording was exported as Microsoft excel sheet. 6-12 wells were analyzed per condition across two control donor hiPSCs, with 16 electrodes per well for MEA. Data is log-transformed and normalized within each plate, prior to one-way ANOVA with a post hoc Bonferroni multiple comparisons test.

STATEMENT OF ETHICS

Ethical approval was not required because the hiPSC lines, lacking association with any identifying information and widely accessible from a public repository, are thus not considered to be human subject research. Post-mortem brain data are similarly lacking identifiable information and are not considered human subject research.

CONFLICT OF INTEREST STATEMENT

K.J.B is a scientific advisor to Rumi Scientific Inc. and Neuro Pharmaka Inc. All other authors declare no conflicts of interest

FUNDING SOURCES

This work was supported by F31MH130122 (K.G.R), R01MH109897 (K.J.B.), R56MH101454 (K.J.B., L.H.), R01MH123155 (K.J.B.) and R01ES033630 (L.H., K.J.B.), R01MH124839 (L.M.H), R01MH106056 (K.J.B) U01DA047880 (K.J.B), R01DA048279 (K.J.B), DOD TP220451 (K.J.B., L.H.), and by the State of Connecticut, Department of Mental Health and Addiction Services. This publication does not express the views of the Department of Mental Health and Addiction Services or the State of Connecticut.

AUTHOR CONTRIBUTIONS

The paper was written by K.G.R., L.H. and K.J.B., with input from all authors. All high-throughput sequencing data and downstream analyses were performed by K.G.R.; L.D. provided code and guidance in conducting Bayesian colocalization analyses. S.L and M.J performed cue-specific ATAC experiments. S.E.W. performed ATAC-seq analysis. P.M.D performed dose-dependent morphological assays and analysis. M.F.G and K.G.R. performed cell-line clonalization. K.G.R performed MPRA library preparation and MPRA experiments with the assistance of M.F.G, S.C, S.C, and A.S.

DATA AVAILABILITY

All source donor hiPSCs have been deposited at the Rutgers University Cell and DNA Repository (study 160; http://www.nimhstemcells.org/).

Full sequencing data, processed data, and accompanying code reported in this paper will be made available through GEO and Synapse upon publication.

CODE AVAILABILITY

The full analysis pipeline (including code and processed data objects) used for analysis of RNA-seq, ATAC-seq, and MPRA data evaluation will be publicly available through Synapse prior to publication.

REFERENCES

1 Consortium, E. P. An integrated encyclopedia of DNA elements in the human genome. *Nature* **489**, 57-74 (2012). https://doi.org/10.1038/nature11247

2 Gerstein, M. B. *et al.* Architecture of the human regulatory network derived from ENCODE data. *Nature* **489**, 91-100 (2012). https://doi.org/10.1038/nature11245

3 Huisman, S. M. H. *et al.* BrainScope: interactive visual exploration of the spatial and temporal human brain transcriptome. *Nucleic Acids Res* **45**, e83 (2017). https://doi.org/10.1093/nar/gkx046

4 Trubetskoy, V. *et al.* Mapping genomic loci implicates genes and synaptic biology in schizophrenia. *Nature* **604**, 502-508 (2022). https://doi.org/10.1038/s41586-022-04434-5

5 O'Connell, K. S. *et al.* Genomics yields biological and phenotypic insights into bipolar disorder. *Nature* **639**, 968-975 (2025). https://doi.org/10.1038/s41586-024-08468-9

6 Grove, J. *et al.* Identification of common genetic risk variants for autism spectrum disorder. *Nat Genet* **51**, 431-444 (2019). https://doi.org/10.1038/s41588-019-0344-8

7 Adams, M. J. *et al.* Trans-ancestry genome-wide study of depression identifies 697 associations implicating cell types and pharmacotherapies. *Cell* **188**, 640-652.e649 (2025). https://doi.org/10.1016/j.cell.2024.12.002

8 Friligkou, E. *et al.* Gene discovery and biological insights into anxiety disorders from a large-scale multi-ancestry genome-wide association study. *Nat Genet* **56**, 2036-2045 (2024). https://doi.org/10.1038/s41588-024-01908-2

9 Nievergelt, C. M. *et al.* Genome-wide association analyses identify 95 risk loci and provide insights into the neurobiology of post-traumatic stress disorder. *Nat Genet* **56**, 792-808 (2024). https://doi.org/10.1038/s41588-024-01707-9

10 Kim, J. J. *et al.* Multi-ancestry genome-wide association meta-analysis of Parkinson's disease. *Nat Genet* **56**, 27-36 (2024). https://doi.org/10.1038/s41588-023-01584-8

11 Bellenguez, C. *et al.* New insights into the genetic etiology of Alzheimer's disease and related dementias. *Nat Genet* **54**, 412-436 (2022). https://doi.org/10.1038/s41588-022-01024-z

12 Uffelmann, E. *et al.* Genome-wide association studies. *Nature Reviews Methods Primers* **1**, 59 (2021). https://doi.org/10.1038/s43586-021-00056-9

13 Abdellaoui, A., Yengo, L., Verweij, K. J. H. & Visscher, P. M. 15 years of GWAS discovery: Realizing the promise. *Am J Hum Genet* **110**, 179-194 (2023). https://doi.org/10.1016/j.ajhg.2022.12.011

14 Cirnigliaro, M. *et al.* The contributions of rare inherited and polygenic risk to ASD in multiplex families. *Proc Natl Acad Sci U S A* **120**, e2215632120 (2023). https://doi.org/10.1073/pnas.2215632120

15 Antaki, D. *et al.* A phenotypic spectrum of autism is attributable to the combined effects of rare variants, polygenic risk and sex. *Nat Genet* **54**, 1284-1292 (2022). https://doi.org/10.1038/s41588-022-01064-5

16 Lipkin, W. I., Bresnahan, M. & Susser, E. Cohort-guided insights into gene-environment interactions in autism spectrum disorders. *Nat Rev Neurol* **19**, 118-125 (2023). https://doi.org/10.1038/s41582-022-00764-0

17 Estes, M. L. & McAllister, A. K. Maternal immune activation: Implications for neuropsychiatric disorders. *Science* **353**, 772-777 (2016). https://doi.org/10.1126/science.aag3194

18 Al-Haddad, B. J. S. *et al.* Long-term Risk of Neuropsychiatric Disease After Exposure to Infection In Utero. *JAMA Psychiatry* **76**, 594-602 (2019). https://doi.org/10.1001/jamapsychiatry.2019.0029

19 Wu, Y., De Asis-Cruz, J. & Limperopoulos, C. Brain structural and functional outcomes in the offspring of women experiencing psychological distress during pregnancy. *Mol Psychiatry* **29**, 2223-2240 (2024). https://doi.org/10.1038/s41380-024-02449-0

20 Han, V. X., Patel, S., Jones, H. F. & Dale, R. C. Maternal immune activation and neuroinflammation in human neurodevelopmental disorders. *Nat Rev Neurol* **17**, 564-579 (2021). https://doi.org/10.1038/s41582-021-00530-8

21 Neuhaus, Z. F. *et al.* Maternal obesity and long-term neuropsychiatric morbidity of the offspring. *Arch Gynecol Obstet* **301**, 143-149 (2020). https://doi.org/10.1007/s00404-020-05432-6

22 Kong, L., Nilsson, I. A. K., Brismar, K., Gissler, M. & Lavebratt, C. Associations of Different Types of Maternal Diabetes and Body Mass Index With Offspring Psychiatric Disorders. *JAMA Netw Open* **3**, e1920787 (2020). https://doi.org/10.1001/jamanetworkopen.2019.20787

23 Smith, S. E., Li, J., Garbett, K., Mirnics, K. & Patterson, P. H. Maternal immune activation alters fetal brain development through interleukin-6. *J Neurosci* **27**, 10695-10702 (2007). https://doi.org/10.1523/JNEUROSCI.2178-07.2007

24 Hsiao, E. Y., McBride, S. W., Chow, J., Mazmanian, S. K. & Patterson, P. H. Modeling an autism risk factor in mice leads to permanent immune dysregulation. *Proc Natl Acad Sci U S A* **109**, 12776-12781 (2012). https://doi.org/10.1073/pnas.1202556109

25 Choi, G. B. *et al.* The maternal interleukin-17a pathway in mice promotes autism-like phenotypes in offspring. *Science* **351**, 933-939 (2016). https://doi.org/10.1126/science.aad0314

26 Kim, E. *et al.* Maternal gut bacteria drive intestinal inflammation in offspring with neurodevelopmental disorders by altering the chromatin landscape of CD4(+) T cells. *Immunity* **55**, 145-158 e147 (2022). https://doi.org/10.1016/j.immuni.2021.11.005

27 Garbett, K. A., Hsiao, E. Y., Kalman, S., Patterson, P. H. & Mirnics, K. Effects of maternal immune activation on gene expression patterns in the fetal brain. *Translational psychiatry* **2**, e98 (2012). https://doi.org/10.1038/tp.2012.24

28 Gallagher, D. *et al.* Transient maternal IL-6 mediates long-lasting changes in neural stem cell pools by deregulating an endogenous self-renewal pathway. *Cell stem cell* **13**, 564-576 (2013). https://doi.org/10.1016/j.stem.2013.10.002

29 Lombardo, M. V. *et al.* Maternal immune activation dysregulation of the fetal brain transcriptome and relevance to the pathophysiology of autism spectrum disorder. *Mol Psychiatry* **23**, 1001-1013 (2018). https://doi.org/10.1038/mp.2017.15

30 Griego, E., Segura-Villalobos, D., Lamas, M. & Galvan, E. J. Maternal immune activation increases excitability via downregulation of A-type potassium channels

and reduces dendritic complexity of hippocampal neurons of the offspring. *Brain Behav Immun* **105**, 67-81 (2022). https://doi.org/10.1016/j.bbi.2022.07.005

31 Sarieva, K. *et al.* Pluripotent stem cell-derived neural progenitor cells can be used to model effects of IL-6 on human neurodevelopment. *Dis Model Mech* **16** (2023). https://doi.org/10.1242/dmm.050306

32 Sarieva, K. *et al.* Human brain organoid model of maternal immune activation identifies radial glia cells as selectively vulnerable. *Mol Psychiatry* **28**, 5077-5089 (2023). https://doi.org/10.1038/s41380-023-01997-1

33 Goshi, N. *et al.* Direct effects of prolonged TNF-alpha and IL-6 exposure on neural activity in human iPSC-derived neuron-astrocyte co-cultures. *Frontiers in cellular neuroscience* **19**, 1512591 (2025). https://doi.org/10.3389/fncel.2025.1512591

34 Yockey, L. J. *et al.* Type I interferons instigate fetal demise after Zika virus infection. *Sci Immunol* **3** (2018). https://doi.org/10.1126/sciimmunol.aao1680

35 Crow, Y. J. & Manel, N. Aicardi-Goutieres syndrome and the type I interferonopathies. *Nat Rev Immunol* **15**, 429-440 (2015). https://doi.org/10.1038/nri3850

36 Fu, J. *et al.* Unraveling the regulatory mechanisms underlying tissue-dependent genetic variation of gene expression. *PLoS genetics* **8**, e1002431 (2012). https://doi.org/10.1371/journal.pgen.1002431

37 GTEx Consortium, Battle, A., Brown, C. D., Engelhardt, B. E. & Montgomery, S. B. Genetic effects on gene expression across human tissues. *Nature* **550**, 204-213 (2017). https://doi.org/10.1038/nature24277

38 Ota, M. *et al.* Dynamic landscape of immune cell-specific gene regulation in immune-mediated diseases. *Cell* **184**, 3006-3021 e3017 (2021). https://doi.org/10.1016/j.cell.2021.03.056

39 Moore, S. R. *et al.* Sex differences in the genetic regulation of the blood transcriptome response to glucocorticoid receptor activation. *Translational psychiatry* **11**, 632 (2021). https://doi.org/10.1038/s41398-021-01756-2

40 Yao, C. *et al.* Sex- and age-interacting eQTLs in human complex diseases. *Hum Mol Genet* **23**, 1947-1956 (2014). https://doi.org/10.1093/hmg/ddt582

41 Linden, M. *et al.* Sex influences eQTL effects of SLE and Sjogren's syndrome-associated genetic polymorphisms. *Biol Sex Differ* **8**, 34 (2017). https://doi.org/10.1186/s13293-017-0153-7

42 Werling, D. M. *et al.* Whole-Genome and RNA Sequencing Reveal Variation and Transcriptomic Coordination in the Developing Human Prefrontal Cortex. *Cell reports* **31**, 107489 (2020). https://doi.org/10.1016/j.celrep.2020.03.053

43 Cuomo, A. S. E. *et al.* Single-cell RNA-sequencing of differentiating iPS cells reveals dynamic genetic effects on gene expression. *Nat Commun* **11**, 810 (2020). https://doi.org/10.1038/s41467-020-14457-z

44 Strober, B. J. *et al.* Dynamic genetic regulation of gene expression during cellular differentiation. *Science* **364**, 1287-1290 (2019). https://doi.org/10.1126/science.aaw0040

45 Elorbany, R. *et al.* Single-cell sequencing reveals lineage-specific dynamic genetic regulation of gene expression during human cardiomyocyte

differentiation. *PLoS genetics* **18**, e1009666 (2022). https://doi.org/10.1371/journal.pgen.1009666

46 Seah, C. *et al.* Common genetic variation impacts stress response in the brain. *bioRxiv*, 2023.2012.2027.573459 (2023). https://doi.org/10.1101/2023.12.27.573459

47 Seah, C. *et al.* Modeling gene x environment interactions in PTSD using human neurons reveals diagnosis-specific glucocorticoid-induced gene expression. *Nat Neurosci* **25**, 1434-1445 (2022). https://doi.org/10.1038/s41593-022-01161-y

48 Davenport, E. E. *et al.* Discovering in vivo cytokine-eQTL interactions from a lupus clinical trial. *Genome biology* **19**, 168 (2018). https://doi.org/10.1186/s13059-018-1560-8

49 Hu, S. *et al.* Inflammation status modulates the effect of host genetic variation on intestinal gene expression in inflammatory bowel disease. *Nat Commun* **12**, 1122 (2021). https://doi.org/10.1038/s41467-021-21458-z

50 Signer, R. *et al.* BMI Interacts with the Genome to Regulate Gene Expression Globally, with Emphasis in the Brain and Gut. *medRxiv* (2024). https://doi.org/10.1101/2024.11.26.24317923

51 Knowles, D. A. *et al.* Determining the genetic basis of anthracycline-cardiotoxicity by molecular response QTL mapping in induced cardiomyocytes. *Elife* **7** (2018). https://doi.org/10.7554/eLife.33480

52 Zhong, Y. *et al.* Leveraging drug perturbation to reveal genetic regulators of hepatic gene expression in African Americans. *Am J Hum Genet* **110**, 58-70 (2023). https://doi.org/10.1016/j.ajhg.2022.12.005

53 Wolter, J. M. *et al.* Cellular Genome-wide Association Study Identifies Common Genetic Variation Influencing Lithium-Induced Neural Progenitor Proliferation. *Biol Psychiatry* **93**, 8-17 (2023). https://doi.org/10.1016/j.biopsych.2022.08.014

54 Tewhey, R. *et al.* Direct Identification of Hundreds of Expression-Modulating Variants using a Multiplexed Reporter Assay. *Cell* **165**, 1519-1529 (2016). https://doi.org/10.1016/j.cell.2016.04.027

55 Inoue, F., Kreimer, A., Ashuach, T., Ahituv, N. & Yosef, N. Identification and Massively Parallel Characterization of Regulatory Elements Driving Neural Induction. *Cell stem cell* **25**, 713-727 e710 (2019). https://doi.org/10.1016/j.stem.2019.09.010

56 Rummel, C. K. *et al.* Massively parallel functional dissection of schizophrenia-associated noncoding genetic variants. *Cell* **186**, 5165-5182 e5133 (2023). https://doi.org/10.1016/j.cell.2023.09.015

57 McAfee, J. C. *et al.* Systematic investigation of allelic regulatory activity of schizophrenia-associated common variants. *Cell Genom* **3**, 100404 (2023). https://doi.org/10.1016/j.xgen.2023.100404

58 Lee, S. *et al.* Massively parallel reporter assay investigates shared genetic variants of eight psychiatric disorders. *Cell* **188**, 1409-1424 e1421 (2025). https://doi.org/10.1016/j.cell.2024.12.022

59 Zhang, Y. *et al.* Rapid single-step induction of functional neurons from human pluripotent stem cells. *Neuron* **78**, 785-798 (2013). https://doi.org/10.1016/j.neuron.2013.05.029

60 Ho, S. M. *et al.* Rapid Ngn2-induction of excitatory neurons from hiPSC-derived neural progenitor cells. *Methods* **101**, 113-124 (2016). https://doi.org/10.1016/j.ymeth.2015.11.019

61 Nehme, R. *et al.* Combining NGN2 Programming with Developmental Patterning Generates Human Excitatory Neurons with NMDAR-Mediated Synaptic Transmission. *Cell reports* **23**, 2509-2523 (2018). https://doi.org/10.1016/j.celrep.2018.04.066

62 Zheng, L. S. *et al.* Mechanisms for interferon-alpha-induced depression and neural stem cell dysfunction. *Stem Cell Reports* **3**, 73-84 (2014). https://doi.org/10.1016/j.stemcr.2014.05.015

63 Rose-John, S., Jenkins, B. J., Garbers, C., Moll, J. M. & Scheller, J. Targeting IL-6 trans-signalling: past, present and future prospects. *Nat Rev Immunol* **23**, 666-681 (2023). https://doi.org/10.1038/s41577-023-00856-y

64 Couch, A. C. M. *et al.* Acute IL-6 exposure triggers canonical IL6Ra signaling in hiPSC microglia, but not neural progenitor cells. *Brain Behav Immun* **110**, 43-59 (2023). https://doi.org/10.1016/j.bbi.2023.02.007

65 Yvanka de Soysa, T., Therrien, M., Walker, A. C. & Stevens, B. Redefining microglia states: Lessons and limits of human and mouse models to study microglia states in neurodegenerative diseases. *Semin Immunol* **60**, 101651 (2022). https://doi.org/10.1016/j.smim.2022.101651

66 Sofroniew, M. V. Astrocyte Reactivity: Subtypes, States, and Functions in CNS Innate Immunity. *Trends Immunol* **41**, 758-770 (2020). https://doi.org/10.1016/j.it.2020.07.004

67 Laighneach, A., Desbonnet, L., Kelly, J. P., Donohoe, G. & Morris, D. W. Meta-Analysis of Brain Gene Expression Data from Mouse Model Studies of Maternal Immune Activation Using Poly(I:C). *Genes (Basel)* **12** (2021). https://doi.org/10.3390/genes12091363

68 Marioni, R. E. *et al.* GWAS on family history of Alzheimer's disease. *Translational psychiatry* **8**, 99 (2018). https://doi.org/10.1038/s41398-018-0150-6

69 Demontis, D. *et al.* Discovery of the first genome-wide significant risk loci for attention deficit/hyperactivity disorder. *Nat Genet* **51**, 63-75 (2019). https://doi.org/10.1038/s41588-018-0269-7

70 Watson, H. J. *et al.* Genome-wide association study identifies eight risk loci and implicates metabo-psychiatric origins for anorexia nervosa. *Nat Genet* **51**, 1207-1214 (2019). https://doi.org/10.1038/s41588-019-0439-2

71 Grove, J. *et al.* Common risk variants identified in autism spectrum disorder. *bioRxiv* (2017). https://doi.org/10.1101/224774

72 Mullins, N. *et al.* Genome-wide association study of more than 40,000 bipolar disorder cases provides new insights into the underlying biology. *Nat Genet* **53**, 817-829 (2021). https://doi.org/10.1038/s41588-021-00857-4

73 Howard, D. M. *et al.* Genome-wide meta-analysis of depression identifies 102 independent variants and highlights the importance of the prefrontal brain regions. *Nat Neurosci* **22**, 343-352 (2019). https://doi.org/10.1038/s41593-018-0326-7

74 International Obsessive Compulsive Disorder Foundation Genetics, C. & Studies, O. C. D. C. G. A. Revealing the complex genetic architecture of obsessive-

compulsive disorder using meta-analysis. *Mol Psychiatry* **23**, 1181-1188 (2018). https://doi.org/10.1038/mp.2017.154

75 Huckins, L. M. *et al.* Analysis of Genetically Regulated Gene Expression Identifies a Prefrontal PTSD Gene, SNRNP35, Specific to Military Cohorts. *Cell reports* **31**, 107716 (2020). https://doi.org/10.1016/j.celrep.2020.107716

76 Lo, M. T. *et al.* Genome-wide analyses for personality traits identify six genomic loci and show correlations with psychiatric disorders. *Nat Genet* **49**, 152-156 (2017). https://doi.org/10.1038/ng.3736

77 Fromer, M. *et al.* Gene expression elucidates functional impact of polygenic risk for schizophrenia. *Nat Neurosci* **19**, 1442-1453 (2016). https://doi.org/10.1038/nn.4399

78 Dobbyn, A. *et al.* Landscape of Conditional eQTL in Dorsolateral Prefrontal Cortex and Co-localization with Schizophrenia GWAS. *Am J Hum Genet* **102**, 1169-1184 (2018). https://doi.org/10.1016/j.ajhg.2018.04.011

79 Barbeira, A. N. *et al.* Exploring the phenotypic consequences of tissue specific gene expression variation inferred from GWAS summary statistics. *Nature Communications* **9** (2018). https://doi.org/10.1038/s41467-018-03621-1

80 Myint, L. *et al.* A screen of 1,049 schizophrenia and 30 Alzheimer's-associated variants for regulatory potential. *Am J Med Genet B Neuropsychiatr Genet* **183**, 61-73 (2020). https://doi.org/10.1002/ajmg.b.32761

81 Ashuach, T. *et al.* MPRAnalyze: statistical framework for massively parallel reporter assays. *Genome biology* **20**, 183 (2019). https://doi.org/10.1186/s13059-019-1787-z

82 O'Brien, H. E. *et al.* Expression quantitative trait loci in the developing human brain and their enrichment in neuropsychiatric disorders. *Genome biology* **19**, 194 (2018). https://doi.org/10.1186/s13059-018-1567-1

83 Bryois, J. *et al.* Cell-type-specific cis-eQTLs in eight human brain cell types identify novel risk genes for psychiatric and neurological disorders. *Nat Neurosci* **25**, 1104-1112 (2022). https://doi.org/10.1038/s41593-022-01128-z

84 Grossman, S. R. *et al.* Systematic dissection of genomic features determining transcription factor binding and enhancer function. *Proc Natl Acad Sci U S A* **114**, E1291-E1300 (2017). https://doi.org/10.1073/pnas.1621150114

85 Liang, D. *et al.* Cell-type-specific effects of genetic variation on chromatin accessibility during human neuronal differentiation. *Nat Neurosci* **24**, 941-953 (2021). https://doi.org/10.1038/s41593-021-00858-w

86 Fulco, C. P. *et al.* Activity-by-contact model of enhancer-promoter regulation from thousands of CRISPR perturbations. *Nat Genet* **51**, 1664-1669 (2019). https://doi.org/10.1038/s41588-019-0538-0

87 Hecker, D., Behjati Ardakani, F., Karollus, A., Gagneur, J. & Schulz, M. H. The adapted Activity-By-Contact model for enhancer-gene assignment and its application to single-cell data. *Bioinformatics* **39** (2023). https://doi.org/10.1093/bioinformatics/btad062

88 de Leeuw, C. A., Mooij, J. M., Heskes, T. & Posthuma, D. MAGMA: generalized gene-set analysis of GWAS data. *PLoS Comput Biol* **11**, e1004219 (2015). https://doi.org/10.1371/journal.pcbi.1004219

89 Consortium, G. T. The GTEx Consortium atlas of genetic regulatory effects across human tissues. *Science* **369**, 1318-1330 (2020). https://doi.org/10.1126/science.aaz1776

90 Yockey, L. J. & Iwasaki, A. Interferons and Proinflammatory Cytokines in Pregnancy and Fetal Development. *Immunity* **49**, 397-412 (2018). https://doi.org/10.1016/j.immuni.2018.07.017

91 Crow, Y. J. *et al.* Characterization of human disease phenotypes associated with mutations in TREX1, RNASEH2A, RNASEH2B, RNASEH2C, SAMHD1, ADAR, and IFIH1. *Am J Med Genet A* **167A**, 296-312 (2015). https://doi.org/10.1002/ajmg.a.36887

92 Sullivan, K. D. *et al.* Trisomy 21 consistently activates the interferon response. *Elife* **5** (2016). https://doi.org/10.7554/eLife.16220

93 Escoubas, C. C. *et al.* Type-I-interferon-responsive microglia shape cortical development and behavior. *Cell* **187**, 1936-1954 e1924 (2024). https://doi.org/10.1016/j.cell.2024.02.020

94 Kettwig, M. *et al.* Interferon-driven brain phenotype in a mouse model of RNaseT2 deficient leukoencephalopathy. *Nat Commun* **12**, 6530 (2021). https://doi.org/10.1038/s41467-021-26880-x

95 Dumitriu, D. *et al.* Deciduous tooth biomarkers reveal atypical fetal inflammatory regulation in autism spectrum disorder. *iScience* **26**, 106247 (2023). https://doi.org/10.1016/j.isci.2023.106247

96 Than, U. T. T. *et al.* Inflammatory mediators drive neuroinflammation in autism spectrum disorder and cerebral palsy. *Scientific reports* **13**, 22587 (2023). https://doi.org/10.1038/s41598-023-49902-8

97 Mostafavi, S. *et al.* Type I interferon signaling genes in recurrent major depression: increased expression detected by whole-blood RNA sequencing. *Mol Psychiatry* **19**, 1267-1274 (2014). https://doi.org/10.1038/mp.2013.161

98 Suzuki, K. *et al.* Microglial activation in young adults with autism spectrum disorder. *JAMA Psychiatry* **70**, 49-58 (2013). https://doi.org/10.1001/jamapsychiatry.2013.272

99 Crow, Y. J. CNS disease associated with enhanced type I interferon signalling. *The Lancet. Neurology* **23**, 1158-1168 (2024). https://doi.org/10.1016/S1474-4422(24)00263-1

100 Wamsley, B. *et al.* Molecular cascades and cell type-specific signatures in ASD revealed by single-cell genomics. *Science* **384**, eadh2602 (2024). https://doi.org/10.1126/science.adh2602

101 Wu, W. L., Hsiao, E. Y., Yan, Z., Mazmanian, S. K. & Patterson, P. H. The placental interleukin-6 signaling controls fetal brain development and behavior. *Brain Behav Immun* **62**, 11-23 (2017). https://doi.org/10.1016/j.bbi.2016.11.007

102 Rochfort, K. D. & Cummins, P. M. The blood-brain barrier endothelium: a target for pro-inflammatory cytokines. *Biochem Soc Trans* **43**, 702-706 (2015). https://doi.org/10.1042/BST20140319

103 Braun, E. *et al.* Comprehensive cell atlas of the first-trimester developing human brain. *Science* **382**, eadf1226 (2023). https://doi.org/10.1126/science.adf1226

104 Eze, U. C., Bhaduri, A., Haeussler, M., Nowakowski, T. J. & Kriegstein, A. R. Single-cell atlas of early human brain development highlights heterogeneity of

human neuroepithelial cells and early radial glia. *Nat Neurosci* **24**, 584-594 (2021). https://doi.org/10.1038/s41593-020-00794-1

105 Emani, P. S. *et al.* Single-cell genomics and regulatory networks for 388 human brains. *Science* **384**, eadi5199 (2024). https://doi.org/10.1126/science.adi5199

106 Inoue, F. *et al.* A systematic comparison reveals substantial differences in chromosomal versus episomal encoding of enhancer activity. *Genome Res* **27**, 38-52 (2017). https://doi.org/10.1101/gr.212092.116

107 Kreimer, A. *et al.* Massively parallel reporter perturbation assays uncover temporal regulatory architecture during neural differentiation. *Nat Commun* **13**, 1504 (2022). https://doi.org/10.1038/s41467-022-28659-0

108 Yamamoto, R. *et al.* Tissue-specific impacts of aging and genetics on gene expression patterns in humans. *Nat Commun* **13**, 5803 (2022). https://doi.org/10.1038/s41467-022-33509-0

109 Bryois, J. *et al.* Time-dependent genetic effects on gene expression implicate aging processes. *Genome Res* **27**, 545-552 (2017). https://doi.org/10.1101/gr.207688.116

110 Huh, C. J. *et al.* Maintenance of age in human neurons generated by microRNA-based neuronal conversion of fibroblasts. *Elife* **5** (2016). https://doi.org/10.7554/eLife.18648

111 Mertens, J. *et al.* Directly Reprogrammed Human Neurons Retain Aging-Associated Transcriptomic Signatures and Reveal Age-Related Nucleocytoplasmic Defects. *Cell stem cell* **17**, 705-718 (2015). https://doi.org/10.1016/j.stem.2015.09.001

112 Miller, J. D. *et al.* Human iPSC-based modeling of late-onset disease via progerin-induced aging. *Cell stem cell* **13**, 691-705 (2013). https://doi.org/10.1016/j.stem.2013.11.006

113 Vera, E., Bosco, N. & Studer, L. Generating Late-Onset Human iPSC-Based Disease Models by Inducing Neuronal Age-Related Phenotypes through Telomerase Manipulation. *Cell reports* **17**, 1184-1192 (2016). https://doi.org/10.1016/j.celrep.2016.09.062

114 Riessland, M. *et al.* Loss of SATB1 Induces p21-Dependent Cellular Senescence in Post-mitotic Dopaminergic Neurons. *Cell stem cell* **25**, 514-530 e518 (2019). https://doi.org/10.1016/j.stem.2019.08.013

115 Ciceri, G. *et al.* An epigenetic barrier sets the timing of human neuronal maturation. *Nature* **626**, 881-890 (2024). https://doi.org/10.1038/s41586-023-06984-8

116 Ernst, J. *et al.* Genome-scale high-resolution mapping of activating and repressive nucleotides in regulatory regions. *Nat Biotechnol* **34**, 1180-1190 (2016). https://doi.org/10.1038/nbt.3678

117 Webber, C. Epistasis in Neuropsychiatric Disorders. *Trends Genet* **33**, 256-265 (2017). https://doi.org/10.1016/j.tig.2017.01.009

118 Andreasen, N. C. *et al.* Statistical epistasis and progressive brain change in schizophrenia: an approach for examining the relationships between multiple genes. *Mol Psychiatry* **17**, 1093-1102 (2012). https://doi.org/10.1038/mp.2011.108

119 Sheth, M. U. *et al.* Mapping enhancer-gene regulatory interactions from single-cell data. *bioRxiv*, 2024.2011.2023.624931 (2024). https://doi.org/10.1101/2024.11.23.624931

120 Gasperini, M. *et al.* A Genome-wide Framework for Mapping Gene Regulation via Cellular Genetic Screens. *Cell* **176**, 377-390 e319 (2019). https://doi.org/10.1016/j.cell.2018.11.029

121 Ren, X. *et al.* High-throughput PRIME-editing screens identify functional DNA variants in the human genome. *Mol Cell* **83**, 4633-4645 e4639 (2023). https://doi.org/10.1016/j.molcel.2023.11.021

122 Zhao, S. *et al.* A single-cell massively parallel reporter assay detects cell-type-specific gene regulation. *Nat Genet* **55**, 346-354 (2023). https://doi.org/10.1038/s41588-022-01278-7

123 Wells, M. F. *et al.* Natural variation in gene expression and viral susceptibility revealed by neural progenitor cell villages. *Cell stem cell* **in press** (2023).

124 Mitchell, J. M. *et al.* Mapping genetic effects on cellular phenotypes with "cell villages". *bioRxiv*, 2020.2006.2029.174383 (2020). https://doi.org/10.1101/2020.06.29.174383

125 Gordon, M. G. *et al.* lentiMPRA and MPRAflow for high-throughput functional characterization of gene regulatory elements. *Nat Protoc* **15**, 2387-2412 (2020). https://doi.org/10.1038/s41596-020-0333-5

126 Ghazi, A. R. *et al.* Design tools for MPRA experiments. *Bioinformatics* **34**, 2682-2683 (2018). https://doi.org/10.1093/bioinformatics/bty150

127 Hunt, G. J., Freytag, S., Bahlo, M. & Gagnon-Bartsch, J. A. dtangle: accurate and robust cell type deconvolution. *Bioinformatics* **35**, 2093-2099 (2019). https://doi.org/10.1093/bioinformatics/bty926

128 Dobin, A. *et al.* STAR: ultrafast universal RNA-seq aligner. *Bioinformatics* **29**, 15-21 (2013). https://doi.org/10.1093/bioinformatics/bts635

129 Liao, Y., Smyth, G. K. & Shi, W. featureCounts: an efficient general purpose program for assigning sequence reads to genomic features. *Bioinformatics* **30**, 923-930 (2014). https://doi.org/10.1093/bioinformatics/btt656

130 Leek, J. T., Johnson, W. E., Parker, H. S., Jaffe, A. E. & Storey, J. D. The sva package for removing batch effects and other unwanted variation in high-throughput experiments. *Bioinformatics* **28**, 882-883 (2012). https://doi.org/10.1093/bioinformatics/bts034

131 Hoffman, G. E. & Schadt, E. E. variancePartition: interpreting drivers of variation in complex gene expression studies. *BMC bioinformatics* **17**, 483 (2016). https://doi.org/10.1186/s12859-016-1323-z

132 Ritchie, M. E. *et al.* limma powers differential expression analyses for RNA-sequencing and microarray studies. *Nucleic Acids Res* **43**, e47 (2015). https://doi.org/10.1093/nar/gkv007

133 Wang, J. & Liao, Y. *WebGestaltR: Gene Set Analysis Toolkit WebGestaltR. R package version 0.4.3.*, <https://CRAN.R-project.org/package=WebGestaltR> (2020).

134 Baines, K. J. *et al.* Maternal Immune Activation Alters Fetal Brain Development and Enhances Proliferation of Neural Precursor Cells in Rats. *Front Immunol* **11**, 1145 (2020). https://doi.org/10.3389/fimmu.2020.01145

135 Dong, Y. *et al.* Transcriptomic profiling of the developing brain revealed cell-type and brain-region specificity in a mouse model of prenatal stress. *BMC Genomics* **24**, 86 (2023). https://doi.org/10.1186/s12864-023-09186-8

136 Willer, C. J., Li, Y. & Abecasis, G. R. METAL: fast and efficient meta-analysis of genomewide association scans. *Bioinformatics* **26**, 2190-2191 (2010). https://doi.org/10.1093/bioinformatics/btq340

137 r/TrimGalore: A wrapper around Cutadapt and FastQC to consistently apply adapter and quality trimming to FastQ files, with extra functionality for RRBS data (GitHub, 2023).

138 Andrews, S. FastQC A Quality Control tool for High Throughput Sequence Data. *Babraham Bioinformatics*

139 Ewels, P., Magnusson, M., Lundin, S. & Kaller, M. MultiQC: summarize analysis results for multiple tools and samples in a single report. *Bioinformatics* **32**, 3047-3048 (2016). https://doi.org/10.1093/bioinformatics/btw354

140 Langmead, B. & Salzberg, S. L. Fast gapped-read alignment with Bowtie 2. *Nat Methods* **9**, 357-359 (2012). https://doi.org/10.1038/nmeth.1923

141 Danecek, P. *et al.* Twelve years of SAMtools and BCFtools. *GigaScience* **10** (2021). https://doi.org/10.1093/gigascience/giab008

142 Zhang, Y. *et al.* Model-based analysis of ChIP-Seq (MACS). *Genome biology* **9**, R137 (2008). https://doi.org/10.1186/gb-2008-9-9-r137

143 Li, Q., Brown, J. B., Huang, H. & Bickel, P. J. Measuring reproducibility of high-throughput experiments. *The Annals of Applied Statistics* **5**, 1752-1779 (2011).

144 Hitz, B. C. *et al.* The ENCODE Uniform Analysis Pipelines. *bioRxiv*, 2023.2004.2004.535623 (2023). https://doi.org/10.1101/2023.04.04.535623

145 Robinson, J. T. *et al.* Integrative genomics viewer. *Nat Biotechnol* **29**, 24-26 (2011). https://doi.org/10.1038/nbt.1754

146 DiffBind: differential binding analysis of ChIP-Seq peak data (Bioconductor, 2021).

147 Heinz, S. *et al.* Simple combinations of lineage-determining transcription factors prime cis-regulatory elements required for macrophage and B cell identities. *Mol Cell* **38**, 576-589 (2010). https://doi.org/10.1016/j.molcel.2010.05.004

148 Yu, G., Wang, L. G. & He, Q. Y. ChIPseeker: an R/Bioconductor package for ChIP peak annotation, comparison and visualization. *Bioinformatics* **31**, 2382-2383 (2015). https://doi.org/10.1093/bioinformatics/btv145

149 Yu, G., Wang, L. G., Han, Y. & He, Q. Y. clusterProfiler: an R package for comparing biological themes among gene clusters. *OMICS* **16**, 284-287 (2012). https://doi.org/10.1089/omi.2011.0118

150 Luo, Y. *et al.* New developments on the Encyclopedia of DNA Elements (ENCODE) data portal. *Nucleic Acids Res* **48**, D882-D889 (2020). https://doi.org/10.1093/nar/gkz1062

151 Kagda, M. S. *et al.* Data navigation on the ENCODE portal. *arXiv* (2023). https://doi.org/https://doi.org/10.48550/arXiv.2305.00006

152 Zuo, C., Shin, S. & Keles, S. atSNP: Transcription factor binding affinity testing for regulatory SNP detection. *Bioinformatics* **31**, 3353-3355 (2015).

153 Coetzee, S. G., Coetzee, G. A. & Hazelett, D. J. motifbreakR: an R/Bioconductor package for predicting variant effects at transcription factor binding sites.

Bioinformatics **31**, 3847-3849 (2015). https://doi.org/10.1093/bioinformatics/btv470

154 Rajarajan, P. *et al.* Neuron-specific signatures in the chromosomal connectome associated with schizophrenia risk. *Science* **362** (2018). https://doi.org/10.1126/science.aat4311

155 Watanabe, K., Taskesen, E., van Bochoven, A. & Posthuma, D. Functional mapping and annotation of genetic associations with FUMA. *Nat Commun* **8**, 1826 (2017). https://doi.org/10.1038/s41467-017-01261-5

156 Duncan, L. *et al.* Significant Locus and Metabolic Genetic Correlations Revealed in Genome-Wide Association Study of Anorexia Nervosa. *Am J Psychiatry* **174**, 850-858 (2017). https://doi.org/10.1176/appi.ajp.2017.16121402

157 Termorshuizen, J. D. *et al.* Genome-wide association studies of binge-eating behaviour and anorexia nervosa yield insights into the unique and shared biology of eating disorder phenotypes. *medRxiv*, 2025.2001.2031.25321397 (2025). https://doi.org/10.1101/2025.01.31.25321397

158 Matoba, N. *et al.* Common genetic risk variants identified in the SPARK cohort support DDHD2 as a candidate risk gene for autism. *Translational psychiatry* **10**, 265 (2020). https://doi.org/10.1038/s41398-020-00953-9

159 Walters, R. K. *et al.* Transancestral GWAS of alcohol dependence reveals common genetic underpinnings with psychiatric disorders. *Nat Neurosci* **21**, 1656-1669 (2018). https://doi.org/10.1038/s41593-018-0275-1

160 Johnson, E. C. *et al.* A large-scale genome-wide association study meta-analysis of cannabis use disorder. *Lancet Psychiatry* **7**, 1032-1045 (2020). https://doi.org/10.1016/S2215-0366(20)30339-4

161 Nievergelt, C. M. *et al.* International meta-analysis of PTSD genome-wide association studies identifies sex- and ancestry-specific genetic risk loci. *Nat Commun* **10**, 4558 (2019). https://doi.org/10.1038/s41467-019-12576-w

162 Cross-Disorder Group of the Psychiatric Genomics Consortium. Genomic Relationships, Novel Loci, and Pleiotropic Mechanisms across Eight Psychiatric Disorders. *Cell* **179**, 1469-1482 e1411 (2019). https://doi.org/10.1016/j.cell.2019.11.020

163 Yu, D. *et al.* Interrogating the Genetic Determinants of Tourette's Syndrome and Other Tic Disorders Through Genome-Wide Association Studies. *Am J Psychiatry* **176**, 217-227 (2019). https://doi.org/10.1176/appi.ajp.2018.18070857

164 Nalls, M. A. *et al.* Identification of novel risk loci, causal insights, and heritable risk for Parkinson's disease: a meta-analysis of genome-wide association studies. *The Lancet. Neurology* **18**, 1091-1102 (2019). https://doi.org/10.1016/S1474-4422(19)30320-5

165 van Rheenen, W. *et al.* Common and rare variant association analyses in amyotrophic lateral sclerosis identify 15 risk loci with distinct genetic architectures and neuron-specific biology. *Nat Genet* **53**, 1636-1648 (2021). https://doi.org/10.1038/s41588-021-00973-1

166 International Multiple Sclerosis Genetics, C. Multiple sclerosis genomic map implicates peripheral immune cells and microglia in susceptibility. *Science* **365** (2019). https://doi.org/10.1126/science.aav7188

167 International League Against Epilepsy Consortium on Complex, E. GWAS meta-analysis of over 29,000 people with epilepsy identifies 26 risk loci and subtype-specific genetic architecture. *Nat Genet* **55**, 1471-1482 (2023). https://doi.org/10.1038/s41588-023-01485-w

168 Hautakangas, H. *et al.* Genome-wide analysis of 102,084 migraine cases identifies 123 risk loci and subtype-specific risk alleles. *Nat Genet* **54**, 152-160 (2022). https://doi.org/10.1038/s41588-021-00990-0

169 Johnston, K. J. A. *et al.* Genome-wide association study of multisite chronic pain in UK Biobank. *PLoS genetics* **15**, e1008164 (2019). https://doi.org/10.1371/journal.pgen.1008164

170 Wu, Y. *et al.* GWAS of peptic ulcer disease implicates Helicobacter pylori infection, other gastrointestinal disorders and depression. *Nat Commun* **12**, 1146 (2021). https://doi.org/10.1038/s41467-021-21280-7

171 Chiou, J. *et al.* Interpreting type 1 diabetes risk with genetics and single-cell epigenomics. *Nature* **594**, 398-402 (2021). https://doi.org/10.1038/s41586-021-03552-w

172 Mahajan, A. *et al.* Multi-ancestry genetic study of type 2 diabetes highlights the power of diverse populations for discovery and translation. *Nat Genet* **54**, 560-572 (2022). https://doi.org/10.1038/s41588-022-01058-3

173 van Walree, E. S. *et al.* Disentangling Genetic Risks for Metabolic Syndrome. *Diabetes* **71**, 2447-2457 (2022). https://doi.org/10.2337/db22-0478

174 Miyazawa, K. *et al.* Cross-ancestry genome-wide analysis of atrial fibrillation unveils disease biology and enables cardioembolic risk prediction. *Nat Genet* **55**, 187-197 (2023). https://doi.org/10.1038/s41588-022-01284-9

175 Surendran, P. *et al.* Discovery of rare variants associated with blood pressure regulation through meta-analysis of 1.3 million individuals. *Nat Genet* **52**, 1314-1332 (2020). https://doi.org/10.1038/s41588-020-00713-x

176 Speliotes, E. K. *et al.* Association analyses of 249,796 individuals reveal 18 new loci associated with body mass index. *Nat Genet* **42**, 937-948 (2010). https://doi.org/10.1038/ng.686

177 Cuellar-Partida, G. *et al.* Genome-wide association study identifies 48 common genetic variants associated with handedness. *Nat Hum Behav* **5**, 59-70 (2021). https://doi.org/10.1038/s41562-020-00956-y

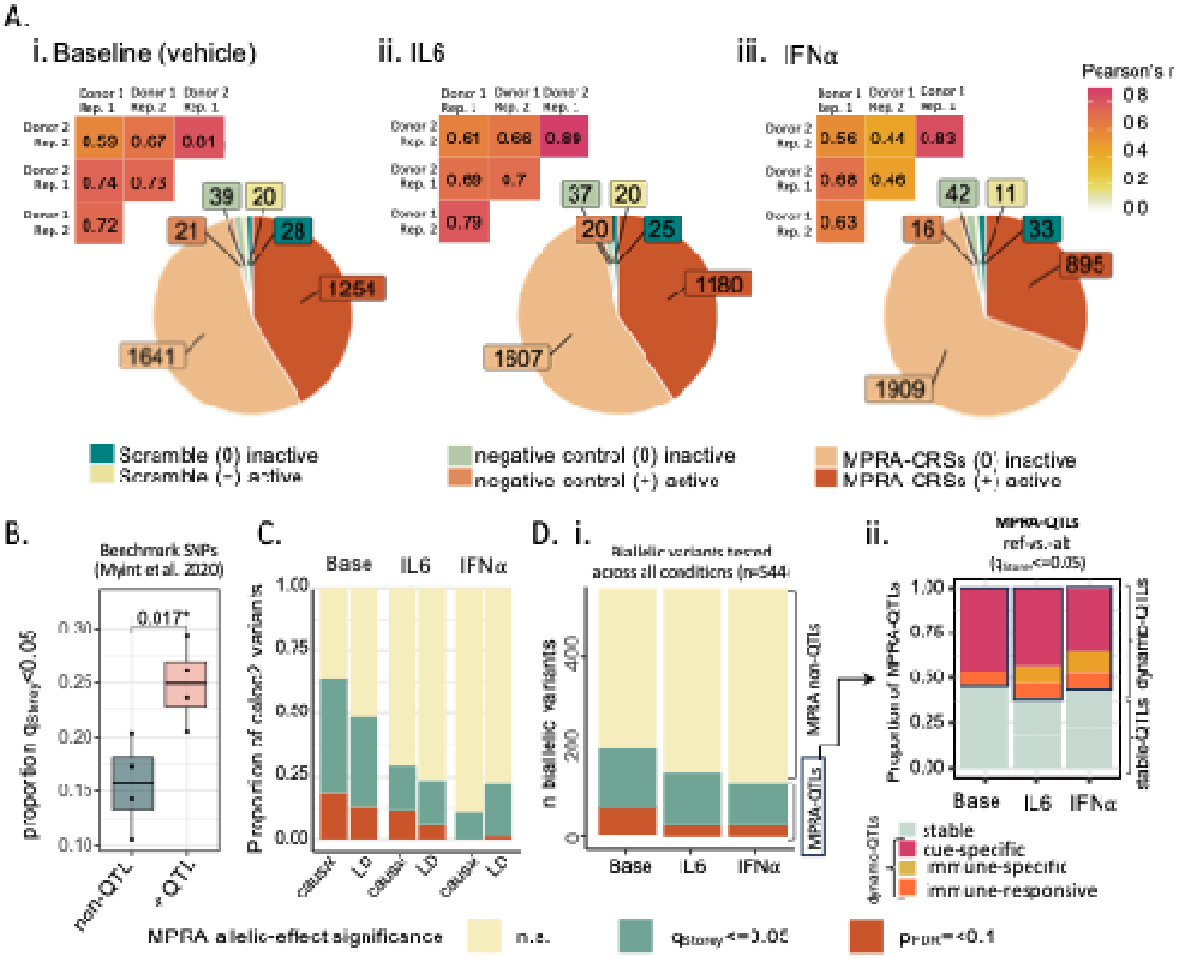

Figure 1. Dynamic immune-responsive neuronal MPRA-QTLs, related to SI Fig. 10-15, SI Data 2.1-2.14. (A) Mature hiPSC-derived glutamatergic neurons (iGLUTs; 2 neurotypical donors/2 replicates) transduced with cross-disorder/trait lenti-MPRA treated with **(i)** 60ng/mL IL-6, **(ii)** 500 IU/mL IFNα-2B, or **(iii)** vehicle (UltraClear-H2O or 0.1% FBS) for 48hrs. Top left: Following QC and filtering, MPRA activity was strongly correlated (Pearson's Correlation Coefficient) across biological (donor 1 – donor 2) and technical replicate (rep.1 – rep. 2) within each condition. Bottom right: Pie chart representing the number of active CREs by condition. Active MPRA-CRSs were identified as those with a transcriptional rate greater than the average activity of scramble control sequences (representing the baseline rate of the minimal promoter). Active MPRA-CRSs most frequently overlapped with excitatory regulatory elements and distal enhancer-like sequences **(SI Fig. 12). (B)** Across conditions, the proportion of experimental positive benchmark variants[80] identified as MPRA-QTLs (bi-allelic sequences with significant ref-v-alt difference in activity) was significantly greater than for negative benchmark variants[80] (Student's T-Test, p-value=0.017). **(C)** Putative causal SNPs (GWAS-eQTL colocalization) were more often MPRA-QTLs relative to SNPs in high LD at baseline (R2=0.8). **(D) (i)** The greatest number of active MPRA-QTLs (n=544) occurred at baseline; across conditions, 23-35% of tested variants were

MPRA-QTLs (q_{Storey}<=0.05) (teal q_{Storey} <=0.05 threshold; terracotta; p_{FDR}<=0.1 threshold). **(ii)** 56-61% of MPRA-QTLs (q_{Storey} <=0.05) were dynamically regulated in response to immune cues most of these (46% of dynamic MPRA-QTLs) were only significant in one condition (cue-specific), whereas 9-12% were significant with the same direction of effect in response to both IL-6 and IFNα (immune-specific) and 8-9% were significant in each condition but with variable directions of effect (immune-responsive). Despite a high percentage of cue-specific QTLs, allelic effects are highly correlated across conditions (Base-v-IL-6: r=0.72, $p=3.5x10^{-13}$; Base-v-IFNα: r=0.69, $p=1.3x10^{-11}$), suggesting that immune cues buffer the magnitude of effect more frequently than changing the direction **(SI Fig. 15B).**

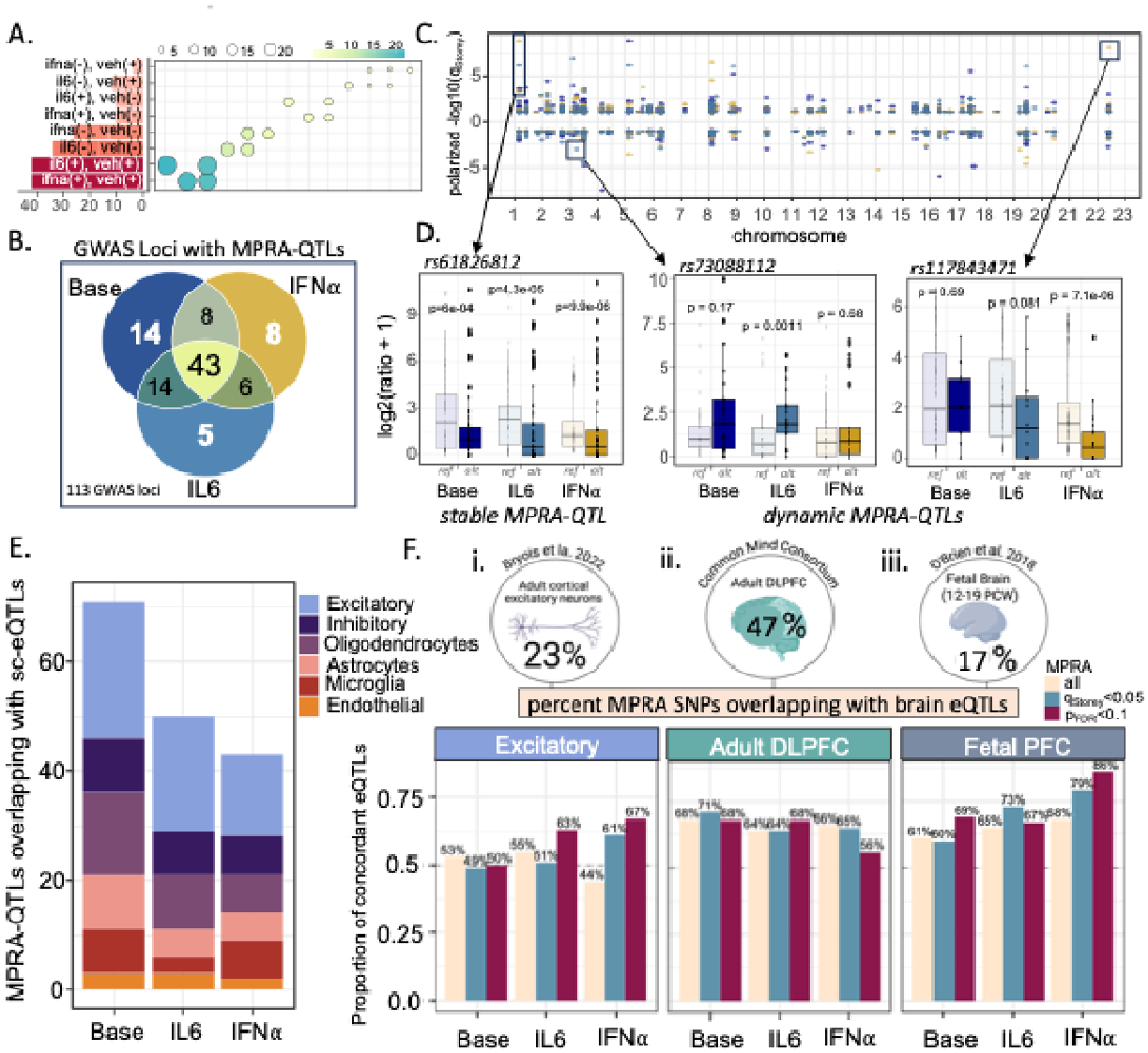

Figure 2. Neuronal MPRA-QTLs largely validate brain eQTLs across inflammatory exposures, related to SI Fig. 17, SI Data 2.16. (A) Upset plot of the overlapping MPRA-QTLs by condition and direction of effect when compared to baseline (vehicle). Within MPRA-QTLs, stable-QTLs generally had increased transcriptional activity with the reference allele. **(B)** Cue-responsiveness often affects the "top" significant QTL at a GWAS locus. While the majority (43 out of 113) of GWAS loci represented had at least one MPRA-QTL in each condition, MPRA-QTLs uniquely mapped to 14 loci at baseline (vehicle), 5 loci for IL-6, and 8 loci for IFNα**. (C)** Genome-wide significant GWAS loci with one or more MPRA-QTL across conditions. **(D) (i)** Representative stable MPRA-QTL: rs61826812 on chromosome 1, with decreased activity with the presence of the alternative allele across all conditions (within condition Wilcoxon Rank Sum test (ref-vs-alt): Base $p=6x10^{-04}$, IL-6 $p=4.3x10^{-05}$, IFNα $p=9.9x10^{-06}$). **(ii-iii)** Representative dynamic MPRA-QTLs: rs73088223 on chr 3 (ii), with increased activity with the alternative allele (p=0.0011) following exposure to IL-6 and rs117843471 on chr 22 (iii) with significant

down regulation with the alternative allele following exposure to IFNα ($p=7.1x10^{-06}$). **(E)** At the single cell level, most MPRA-QTLs overlapped with excitatory neuronal QTLs[83], as anticipated. **(F)** Of the 544 bi-allelic variants tested, 23%, 47%, and 17% percent overlapped with significant (Bonferroni or FDR<=0.05) **(i)** adult cortical excitatory neuronal[83], **(ii)** adult brain[77], and **(iii)** fetal brain (12-19 PCW[82]) eQTLs, respectively. The concordance of allelic effects (ref-v-alt) was tested across all MPRA bi-allelic variants overlapping with brain eQTLs (cream bar), MPRA-QTLs at a q_{Storey}<=0.05 threshold (teal bar), and MPRA-QTLs at p_{FDR}<=0.1 threshold. The magnitude of effect of these concordant MPRA-QTLs was also significantly correlated with eQTL betas (**SI Data 2.16**): MPRA-QTLs q_{Storey} <=0.05: (Excitatory: r=0.5-0.71; DLPFC: r=0.64-0.66; Fetal PFC: r=0.71-0.82)].

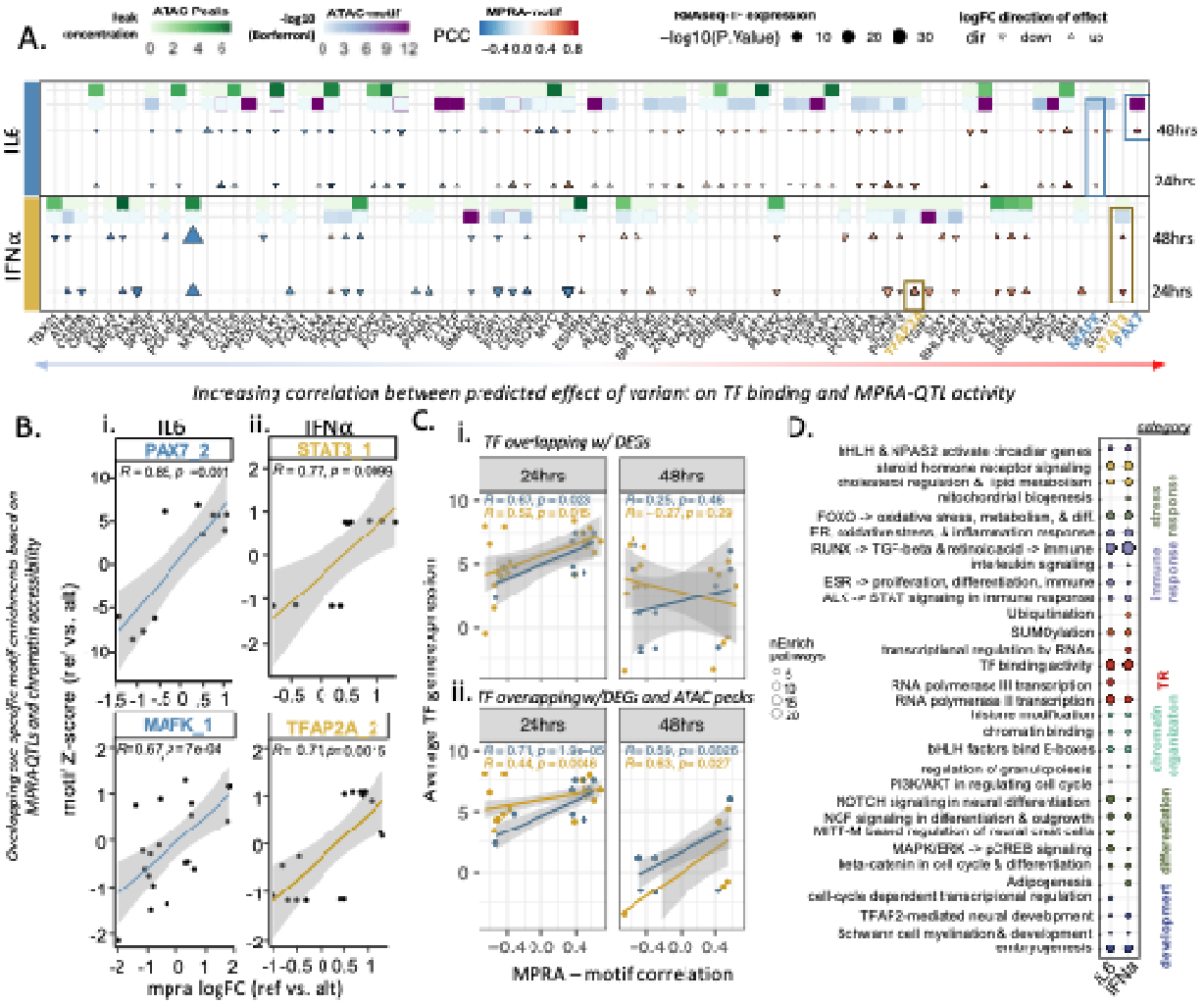

Figure 3. Dynamic regulation is likely driven by variant-specific binding affinities and cue-specific changes in chromatin accessibility, related to SI Fig. 18, SI Data 2.18. Allele-specific effects on transcription factor (TF) binding affinities were tested across 1573 binding motifs representing 446 TFs expressed in mature iGLUTs. To identify TF regulating a large proportion of MPRA-QTLs, we compared the measured allelic effects across MPRA-QTLs (q_{Storey} <0.05) and affinity binding z-scores based on TF motif-SNP interactions with predicted difference in binding based on variant (q_{Storey} <0.05). Top TF motifs positively correlated with enhancer activity were largely unique across conditions. **(A)** Many of the top predicted MPRA-QTL regulating transcription factors overlapped with motif enrichments based on chromatin accessibility in donor matched mature iGLUTs exposed to vehicle, IL-6, or IFNα (cue-specific ATAC peaks) and showed differential gene expression patterns following treatment with IL-6 and IFNα, which were temporally dynamic (24hrs-vs-48hrs). Dot plot and heatmap representing top TFs predicted to regulate cue-specific MPRA-QTL that either overlapped with differentially accessible ATAC peaks (cue-vs-vehicle) (green; color=Peak concentration), ATAC motif enrichments (purple; color=-log10(p_{Bon})) or differentially expressed genes (size=-log10(P-value), shape=direction of logFC (up or

down regulated), with the Pearson's Correlation Coefficient as the fill of each dot (blue=negative correlation; red=positive) and TFs organized by magnitude of correlation. **(B)** PAX7_2 (r=0.85, p=0.001) and MAFK_1 (r=0.67, $p=7x10^{-4}$) and STAT3_1 (r=0.77, p<=0.0099) and TFAP2A_2 (r=0.71, p=0.0015) were top correlated motifs at following IL-6 and IFNα exposure respectively; individual SNPs represented as points (R=Pearson's Correlation Coefficient). **(C)** TF average gene expression was significantly positively correlated with MPRA-motif correlations at 24hrs (IL-6: r=0.67, p=0.023; IFNα: r=0.52, p=0.015), but not at 48hrs **(i).** However, when further filtering for TFs with differential gene expression that also lie in chromatin accessibility peaks, association between average expression and MPRA-motif correlations significantly stronger and present at both 24hrs (IL-6: r=0.71, $p=1.9x10^{-05}$; IFNα: r=0.44, p=0.0046), and 48hrs (IL-6: r=0.59, p=0.0026; IFNα: r=0.63, p=0.027) **(ii). (D)** Comparative over-representation analysis between IL-6 and IFNα associated TF in (A) for Gene Ontology terms and REACTOME pathways. Size represents the total number of unique term enrichments with evidence for affecting a signaling cascade, ordered and colored by broader category.

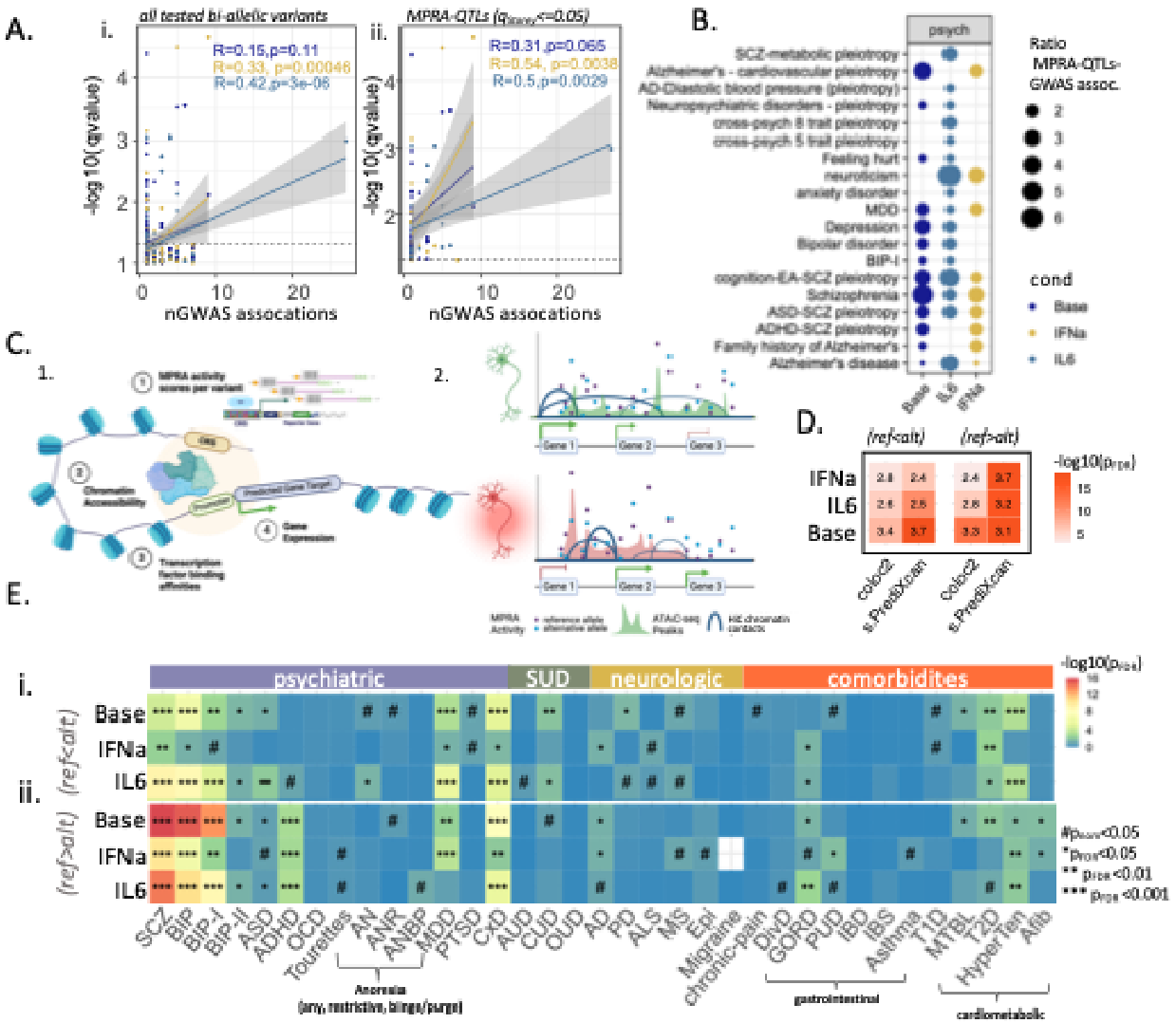

Figure 4. Gene targets of dynamic regulatory elements follow neuronal immune activation show distinct associations with neuropsychiatric traits, psych-psych pleiotropy, and psych-cardiometabolic pleiotropy, related to SI Fig. 19-20; SI Data 2.19-2.22. Across all conditions, MPRA-QTL significance was positively associated with the number of unique GWAS trait associations (GWAS Catalogue; **SI Data 2.19**), with greater correlations between multi-trait associations and MPRA-QTL significance following neuronal immune activation IL-6: all CRSs: r=0.42, p=3x10^{-6}, MPRA-QTLs, r=0.5, p=0.0029; IFNα: all CRSs, r=0.33, p=0.00046, MPRA-QTLs, r=0.54, p=0.0038; Base(Veh.): MPRA- all CRSs, r=0.15, p=0.11; MPRA-QTLs, r=0.21, p=0.065). (B) Many of these MPRA-QTLs indicate cue-specific regulation of psych-psych pleiotropy or psych-cardiometabolic pleiotropy – for example, between IL-6 and SCZ-metabolic pleiotropy and IFNα and Alzheimer's Disease (AD) and cardiovascular pleiotropy. (C) To further explore potential multi-trait and pleiotropic associations of risk variants regulated by cellular inflammation – we performed activity-by-contact (ABC) enhancer-gene interaction scoring (1.) By integrating cue-specific iGLUT MPRA enhancer activity, cue-specific iGLUT chromatin accessibility peaks, iGLUT specific chromatin contact, and transcription factor binding affinities we (2.) predict cue-responsive genetically regulated

genes (ABC genes) specific to the chromatin architecture and gene expression of iGLUTs. (D) ABC gene targets of MPRA-QTLs across conditions both significantly overlap with DLPFC eGenes identified by S-PrediXcan and Coloc2 (hypergeometric enrichment test) and represent loci not predicted by GWAS, colocalization, or transcriptomic imputation. **(E)** Across conditions, MPRA-QTL gene targets were strongly enrichened for SCZ, BIP, cross-disorder pleiotropy, and neuroticism, consistent with the cross-disorder design and larger proportion of prioritized variants from SCZ, BIP, and neuroticism GWAS. Of note, MPRA-QTL target genes were enriched for common psych-comorbidities like T2D, hypertension, and GORD. Enrichments also show cue-specific effects, notably, there is a unique moderate association between IL-6 and Anorexia as well as with each tested neurogenerative/neurological disorder (SD, PD, ALS, MS). Heatmap of MAGMA enrichments across psychiatric, substance use (SUD), neurological, metabolic/autoimmune disorders, and cardiometabolic GWAS, colored by $-\log10(p_{FDR})$ (p_{nom}<=0.05$^{\#}$, p_{FDR} <0.05*, p_{FDR} <0.01**, p_{FDR} <0.001***). *NeuroPsych*: Attention Deficit/Hyperactivity Disorder (ADHD), Anorexia (AN; R - restrictive or BP – binge/purge), Autism Spectrum Disorder (ASD), Bipolar Disorder (BIP), BIP type-1 (BIP-I), BIP type-2 (BIP-II), Cross 8 neuro-psych disorders (CxD), Major Depressive Disorder (MDD), Post-traumatic stress disorder (PTSD) , Obsessive-compulsive Disorder (OCD); *Substance Use Disorders:* Alcohol Use Disorder (AUD); Cannabis Use Disorder (CUD), Opiod Use Disorder (OUD); *Neurological:* Alzheimer's Disease (AD), Parkinson's Disease (PD), Amyotrophic lateral sclerosis (ALS), Multiple Sclerosis (MS), Epilepsy (Epi); *Inflammatory-Gastrointestinal*: Diverticular Disease (DivD), Gastro-oesophageal reflux disease (GORD), Peptic Ulcer Disease (PUD), Inflammatory Bowel Disease (IBD), Irritable Bowel Syndrome (IBS), Asthma, Type-I Diabetes (T1D); *Cardiometabolic*: Metabolic Syndrome (MTBL), Type-2 Diabetes (T2D), Atrial Fibrillation (Afib), hypertension (HyperTen); *Anthropometric:* Body Mass Index (BMI), left-handedness (left hand).

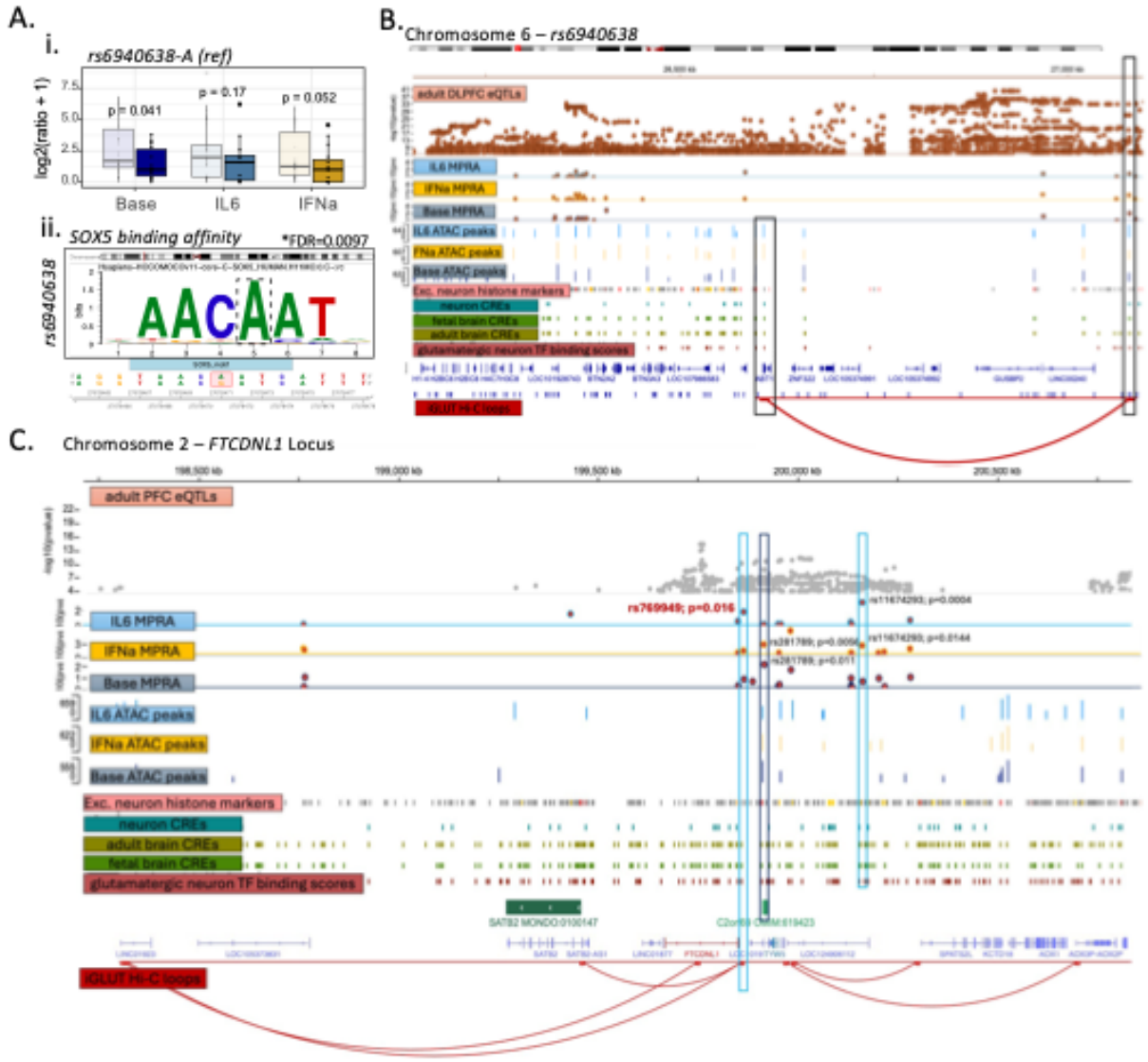

Figure 5. Stable and immune dynamic MPRA-QTLs regulate psychiatric risk genes through neuron specific chromatin contact. (A) (i) rs6940638 is a stable MPRA-QTL across conditions with significantly reduced transcriptional activity with the alternative allele (G) (Wilcoxon Rank Sum Test; Base: p=0.041, IL6=0.17, p=0.052; MPRAnalyze; Base: q_{Storey}=0.01; IL6: q_{Storey}=0.05; IFNa q_{Storey}=0.027). **(ii)** SOX5 binds at this *rs6940638*, with significant increased affinity for the reference allele (A). **(B)** While rs6940638 is associated with intelligence [Intelligence GWAS] and is a brain-QTL of BTN2A/BTN3A3, in iGLUTs ABC prediction models suggest it more strongly regulates *ABT1* – iGLUT chromatin accessibility show that rs6940638 lies in an iGLUT chromatin accessibility peak spanning previously identified brain regulatory elements (PsychENCODE CREs tracks) with positive TF binding activity in neurons, specifically for the SOX5 motif (PsychENCODE). This region is connected by iGLUT-specific chromatin loops to regulatory elements in open chromatin regions 500KB with annotated TF binding activity in neurons (track). **(C)** The FTCDNL1 locus falls under dynamic regulation by multiple MPRA-validated brain-eQTLs (GTeX v8 Frontal Cortex, CMC DLPFC). Notably, rs769949 is a cue-specific MPRA-QTL (IL6: q_{Storey}=0.016;

Frontal Cortex eQTL - *FTCDNL1* $p=4.6x10^{-7}$, *TYW4* $p= 4.8x10^{-6}$) lies in an iGLUT-specific chromatin loop – with predicted multi-gene regulation including *STAB2.*